Published in final edited form as:
Coord Chem Rev. 2015 December 1; 304-305: 3–19. doi:10.1016/j.ccr.2015.03.014.

Recent Developments in Hydrogen Evolving Molecular Cobalt(II)-Polypyridyl Catalysts

N. Queyriaux[a], **R. T. Jane**[a], **J. Massin**[a], **V. Artero**[a,*], and **M. Chavarot-Kerlidou**[a,*]

[a]Laboratoire de Chimie et Biologie des Métaux, Univ. Grenoble Alpes, CNRS UMR 5249, CEA, 17 rue des martyrs, 38054, Grenoble Cedex 9, France

Abstract

The search for efficient noble metal-free hydrogen-evolving catalysts is the subject of intense research activity. A new family of molecular cobalt(II)-polypyridyl catalysts has recently emerged. These catalysts prove more robust under reductive conditions than other cobalt-based systems and display high activities under fully aqueous conditions. This review discusses the design, characterization, and evaluation of these catalysts for electrocatalytic and light-driven hydrogen production. Mechanistic considerations are addressed and structure-catalytic activity relationships identified in order to guide the future design of more efficient catalytic systems.

Keywords

Hydrogen; Cobalt; Polypyridyl ligands; Electrocatalytic activity; Photocatalytic activity

1. Introduction

The conversion of solar energy into chemical energy through light-driven water splitting to produce hydrogen (H_2) may provide a new method of energy delivery based on the exclusive use of renewable resources, water and sunlight. Hydrogen is indeed a carbon free fuel, and possesses the highest energy output relative to mass [1]. Fuel cell technology allows this energy source to be converted into electricity on demand, with very high energy conversion efficiencies and without the production of greenhouse gases. In the context of water splitting, photosynthesis has been a great source of inspiration for the molecular chemistry community, and the design of molecular systems for hydrogen evolution, inspired by the Photosystem I-Hydrogenase couple found in some hydrogen producing photosynthetic micro-organisms [2-4], is at the heart of the field of *artificial photosynthesis* [5-10]. Of particular interest is the fact that the activities of the biological systems rely on first-row transition metals, leading to intense research activity in the field of bio-inspired noble metal-free hydrogen evolution catalysis, which may provide an alternative to the use of rare and expensive metals such as platinum in state of the art technological applications [11-15].

* vincent.artero@cea.fr; murielle.chavarot-kerlidou@cea.fr.

Europe PMC Funders Author Manuscripts

While having no biological relevance for water splitting, cobalt has emerged as a major player in the field in the last ten years [16, 17]. The potential use of cobalt-based catalysts in light-driven hydrogen evolution was identified some time ago [17], yet the cobaloxime catalysts (Scheme 1, **1a-c**) had to wait until the mid-2000s to experience a renewal in interest, thanks to several detailed electrocatalytic studies [18-21]. Numerous efficient homogeneous photocatalytic systems, either multicomponent [22-30] or based on supramolecular photosensitizer-catalyst assemblies [31-39], have since been reported, displaying activity in fully organic or mixed organic-aqueous solutions. However, the cobaloxime catalysts suffer from a low stability, particularly in the reduced state, which limits their long-term efficiency. This drawback has been partly circumvented by substituting the two bidentate dimethylglyoxime ligands (Scheme 1) for the tetradentate diimine dioxime ligand, giving complexes that are more stable toward ligand exchange reactions [40-44].

The 2010s saw the start of a new chapter in the cobalt-based hydrogen production saga, with the first reports on the hydrogen evolution activity of cobalt(II)-polypyridyl complexes. These studies took inspiration from the work of Sutin and coworkers in the 1980s on the cobalt-trisbipyridine complex (Scheme 1, **2**) [45-50]. The polypyridyl catalysts display an increased stability under reductive conditions compared to both the parent $[Co(bpy)_3]^{2+}$ compound and the cobaloximes, thus allowing a more systematic evaluation of their activity in fully aqueous media. This has stimulated the design of new electro- and photocatalytic systems based on cobalt(II)-polypyridyl complexes, particularly in the last four years.

In this review article, the design, characterization, and evaluation of molecular cobalt(II)-polypyridyl catalysts for electrocatalytic and light-driven hydrogen production will be discussed. Structure-catalytic activity relationships will be specifically highlighted in order to define guidelines for the future design of more efficient catalytic systems. For the sake of clarity, classification of the polypyridyl ligands and their corresponding cobalt(II) complexes has been made on the basis of their structural features (and therefore does not follow the chronological order of publication). They have been divided into two families: the bipyridine-based structures (Schemes 2 and 3, ligands **L3a** to **L9**, catalysts **3a** to **9**) and the pyridine-based structures (Scheme 4, ligands **L10a** to **L12b**, catalysts **10a** to **12b**), each family comprising both tetradentate and pentadentate ligands.

2. Electrochemical and electrocatalytic studies

The electrochemical characterization and assessment of the electrocatalytic performance of a catalyst are important steps in catalyst development, benchmarking [51] and understanding. These experiments provide important information about the electrochemical potential and rate at which catalysis occurs, as well as mechanistic details such as the nature of the catalytic process (cobalt-centered *vs* ligand-assisted). Due to their relatively high stability, information about electrocatalytic activity under fully aqueous conditions is almost always available. This can then be used to rationalize the photocatalytic hydrogen evolution activities measured under such conditions, provided both electro- and photocatalytic experiments were performed at the same pH. Additional kinetic and mechanistic information can be obtained by performing electrocatalytic studies in organic media, wherein proton

delivery to the catalyst can be controlled by the addition of precisely measured amounts of a proton source with a given pK_a.

In the following we will describe the different systems, starting with those for which an exclusively cobalt-centered catalytic mechanism is demonstrated. Catalysts exhibiting a ligand-assisted catalytic process will be described in a second part. The electrocatalytic performances of these catalysts are summarized in Table 1. It should be noted that to the best of our knowledge, no electrocatalytic study has been reported for the parent $[Co(bpy)_3]^{2+}$ complex **2**.

2.1. Brief overview of hydrogen evolution mechanisms in cobalt-based catalysts

Hydrogen evolution catalyzed by molecular cobalt complexes generally implies the formation of a cobalt hydride species by protonation of a Co(I) intermediate [17]. The catalytic system may then evolve through two distinct mechanisms. In the heterolytic mechanism (Figure 1), the intermediate metal hydride, either Co(III)–H or Co(II)–H, decomposes by proton attack and evolves hydrogen *via* an intermediate dihydrogen metal σ-complex. During the catalytic cycle, two electrons are thus transferred to the complex, either consecutively (Figure 1, ECCE or EECC pathways, with E corresponding to electron transfer and C to protonation steps) or alternating with the two protonation steps (Figure 1, ECEC pathway). The distinction between these two mechanisms has so far proven very difficult to establish, except in a few cases where the second reduction step occurs at a more cathodic potential than the first [60, 61]. In the case of the well-studied cobaloximes and their diimine dioxime derivatives, DFT calculations favour the heterolytic mechanism involving a Co(II)–H as the intermediate species from which hydrogen is evolved [62-65]. In the alternative mechanism, two metal-hydride complexes evolve hydrogen through a reductive elimination reaction, involving homolysis of the Co–H bonds (homolytic pathways, inset Figure 1). Thus, in the course of the catalytic cycle, each metal center undergoes a single monoelectronic reduction process, either before protonation or once the Co(III)–H species is formed. It is important to note that both pathways can coexist [66], and that switching from a heterolytic to a homolytic pathway can simply be a matter of experimental conditions, such as the relative concentrations of protons and catalysts or acid strength, as recently demonstrated by Costentin and Savéant in the case of an iron-porphyrin catalyst [67]. Of note is the fact that strong acids are required for Co(III)–H species to evolve hydrogen in a heterolytic manner [68].

The exact nature of the hydrogen evolution mechanism has not yet been investigated with the cobalt(II)-polypyridyl catalysts. As for related amino-polypyridinyl cobalt systems [69], a heterolytic mechanism involving a Co(II)–H species is likely, following the conclusions gained from studies on cobaloximes and related compounds. In addition, the introduction of redox-active moieties such as bipyridine [70] in the polypyridyl coordination sphere of the cobalt center has two major consequences: (i) it stabilizes reduced states of the metal center and thus shifts the cobalt-centered reduction process to more positive potentials. As a consequence, the reduced Co(I) state is less basic and therefore less nucleophilic, and thus requires more acidic conditions for cobalt-centered catalysis to occur; (ii) at the same time, it introduces new ligand-centered reduction processes generating $Co(I)(L^{\cdot-})$ species,

sometimes referred to as a formal Co(0) state. This process is observed at potentials less negative than that which would be required to reduce the cobalt center one step further, *i.e.* to the spectroscopic Co(0) state. Protonation of this Co(I)($L^{\cdot-}$) species can then occur, likely generating a Co(II)–H species (Figure 1, EECC pathways) competent for hydrogen generation.

2.2. Cobalt(II)-polypyridyl catalysts displaying exclusively cobalt-centered catalytic processes

The first hydrogen evolving cobalt(II)-polypyridyl electrocatalyst, the octahedral cobalt(II) complex **3b**, was reported in 2010 by Chang and coworkers [52]. These authors designed **L3b** bearing pyridine moieties to stabilize the metal center in its reduced states, and binding in a tetradentate manner, thus leaving two open coordination sites in *cis* position on which substrate binding and catalysis may occur. The cyclic voltammogram of **3b** recorded in acetonitrile displays a reversible cathodic wave at −0.81 V *vs* SCE and a quasi-reversible oxidation at +0.87 V *vs* SCE, assigned to the Co(II/I) and the Co(III/II) couples, respectively. Addition of trifluoroacetic acid (TFA) triggers the appearance of a catalytic wave, near the Co(II/I) couple (the mid-wave of the electrocatalytic wave corresponds to an overpotential for hydrogen production of ~400 mV), attributed to the catalytic reduction of protons. Controlled potential electrolysis experiments at −1.0 V *vs* SCE confirm formation of hydrogen with 99% faradaic yield [52]. The catalytic wave plateaus at high acid concentrations, with catalytic current independent of the scan rate. This indicates that the system operates in the ‘pure kinetic’ catalytic regime with negligible consumption of the substrate (*i.e.* protons) [71]. As expected, the plateau current varies linearly with the concentration of the catalyst **3b**. However, a similar linear variation is found with regards to TFA concentration, indicating that the catalytic rate is second order in acid. Although such a dependency has been observed relatively frequently for other catalysts, including cobalt-based ones [56, 72-75], it does not fit with any of the classical mechanisms for hydrogen evolution [76]. Nevertheless, a turnover frequency (TOF) of 40 mol H_2/mol catalyst/hour at 60 mM TFA could be determined. The catalyst **3b** is not soluble in water in the millimolar range, but the authors were able to demonstrate the compatibility of this polypyridyl platform with aqueous conditions by working in a 50:50 water acetonitrile mixture. Under these conditions, electrocatalytic proton reduction is also triggered by addition of TFA at a potential very close to the Co(II/I) reduction wave (−1.0 V *vs* SCE), with similar current densities to those observed in pure acetonitrile. Of note is a second, possibly catalytic process observed at a slightly more negative potential (−1.2 V *vs* SCE), but which has not been investigated in detail. We note, however, that this behavior, with consecutive catalytic processes, finds equivalence in the electrochemistry of compounds **10** and **11** discussed below. Also of note is the fact that **L3b** contains a bipyridine moiety with potential redox activity.

Water solubility was obtained through modification of the ligand [57]. Catalyst **4a** is closely related to catalyst **3b**, but with a methyl substituent instead of a methoxy group, and a triflate residual ligand on the cobalt center instead of an acetonitrile molecule. Electron-withdrawing groups have also been introduced e.g. in **L4b**, following the observation of the beneficial effect of such substituents on the series of catalyst **11a-c** (see below) [58]. The

cyclic voltammograms of complexes **4a** and **4b** (0.3 mM) were recorded in pH 4 ascorbic acid/ascorbate buffer, the same conditions employed for photocatalytic testing (see section 3.2). Complex **4a** shows electrocatalytic current enhancement at approximately −0.90 V *vs* SHE with no discernible pre-catalytic features. Comparison with **3b** indicates that the onset potential for the electrocatalytic wave corresponds to the reduction of the complex to the Co(I) state. In contrast, **4b** displays a small pre-catalytic feature at −0.75 V *vs* SHE, which has been assigned to the Co(II/I) reduction and is likely non-catalytic. In addition, hydrogen evolution catalyzed by **4b** occurs at potentials more negative than −0.90 V *vs* SHE (**4a**), which contrasts with the trend observed in the series **11a-c** (see below). While no detailed mechanistic data are provided in the original paper, it is tempting to propose that the introduction of the electron-withdrawing group in **L4b** results in the inversion of the redox potentials of the Co(II/I) and the Co(III)–H/Co(II)–H couples of **4b** (the latter triggering catalysis) as compared to the situation found for **4a**. Also of note is the fact that the catalytic current obtained with **4b** is significantly lower than that obtained with **4a**. Indeed, the introduction of electron-withdrawing groups in cobalt polypyridyl complexes often leads to diminished activity of the corresponding Co(I) species [54]. Such a trend is confirmed in photocatalytic assays.

The same group has also synthesized a pentadentate pyridine-based "Py_5Me_2" ligand, **L11**, and first demonstrated the impressively high efficiency and robustness of the oxo- and disulfide-molybdenum complexes of **11b** for hydrogen generation from neutral water [77, 78]. A series of cobalt complexes **11** was subsequently prepared and evaluated in pH 7 phosphate buffer solutions. Two electrocatalytic processes are observed at mercury drop or mercury pool electrodes. The first is peak-shaped and develops at a potential close to the Co(II/I) couple (−1.0 V *vs* SHE for complex **11b**) as independently measured in acetonitrile solutions [7]. The second process occurs at a potential 200 mV more cathodic and seems to be limited only by mass transport of protons to the electrode surface. Controlled potential electrolysis coupled to GC measurements, carried out at a potential below that of the second process (−1.30 V *vs* SHE), established the stability of **11b** during hydrogen evolution, with a 100% faradaic yield and 55000 TONs achieved during a 60 hour experiment. Substitution on the central pyridine ring by either electron-withdrawing (**L11a**) or electron-donating (**L11c**) groups allows for tuning of the potential of both hydrogen evolution processes, highlighting the role of molecular design in catalyst optimization [58]. While no mechanistic information is available for this second process, which possibly involves a Co(0) state, rotating disk electrode (RDE) voltammetry allowed further insights into the first catalytic process in the case of complex **11a** [59]. From the voltammograms obtained at different rotation rates in 0.1 M pH 7 phosphate buffer, a Levich plot was constructed from the current density at −0.9 V *vs* SHE, and its linearity indicates catalysis operating under diffusion control. Despite the fact that no bulk electrolysis experiment has been performed at the exact potential of this first wave, the catalytic nature of the process was demonstrated by comparing the current density measured at −0.9 V *vs* SHE to that of the Co(III/II) process observed at +0.4 V *vs* SHE. This ratio (almost 16) was much higher than the values of 1 to 8 reported for a series of cobalt complexes at a similar overpotential of 500 mV in pH 2.2 aqueous buffer [79]. The cobalt-centered mechanism of proton reduction by catalysts **11** was also investigated in acetonitrile in the presence of acetic acid [55]. Compound **11b** displayed two well-defined

reversible redox events at +0.815 V and −0.830 V *vs* SHE, assigned to the Co(III/II) and Co(II/I) events, respectively. Surprisingly, the addition of acetic acid caused a *decrease* in the current at the Co(II/I) couple and the appearance of a catalytic wave at a slightly more negative potential (−1.10 V *vs* SHE). This behavior could be explained through anation of the complex by the conjugate base produced during catalysis, the acetate anion. Indeed, addition of tetrabutylammonium acetate (*n*-$Bu_4N(OAc)$) to a solution of **11b** in acetonitrile caused the appearance of a new couple at −1.18 V *vs* SHE, with complete disappearance of the original wave after the addition of one equivalent. Furthermore, titration of a 1:1 mixture of *n*-$Bu_4N(OAc)$:AcOH into a solution of **11b** showed the development of a catalytic peak at the potential of the Co(II/I) couple of the acetate-bound species, the peak current *vs* acid concentration demonstrating first order kinetics at all concentrations, while addition of excess *n*-$Bu_4N(OAc)$ to a solution of the acetate complex with acetic acid inhibits catalysis. Addition of acids of various strength to **11b**, and also to the CF_3 (**11a**) and NMe_2-substituted (**11c**) compounds showed that in all cases, current enhancement at the Co(II/I) couple, as well as evidence for anation by the conjugate base, were present in the cyclic voltammograms.

Interestingly, no anation was observed by Scandola and coworkers for the cobalt complex with the "Py_5" ligand **L12b**, with a structure very similar to **L11b**, varying only in the substitution on the methylene linkers [56]. They investigated the electrocatalytic activity of **12b** in acetonitrile in the presence of increasing amounts of TFA, the conjugate of which is expected to be a weaker ligand than acetate. A catalytic wave developed at potential slightly more positive than that of the Co(II/I) redox couple (−1.31 V *vs* SCE) and has been assigned to hydrogen production. It should be noted, however, that no bulk electrolysis experiment coupled to GC measurements is reported in order to confirm the formation of hydrogen. The authors tentatively proposed a mechanism based on the formation of a Co(III)–H intermediate followed by reduction to Co(II)–H. At high acid concentration, however, the observation of catalytic current from very positive potentials (onset at −0.50 V *vs* SCE) suggests detachment and protonation of one of the pyridine groups on the pentadentate ligand, since reduction of the more positively charged protonated complex is expected to occur at a less cathodic potential. Such a mechanism has already been suggested by Wang and coworkers for a related complex [80].

Ligands **L10a-c** are structurally related to ligands **L11a-c**, from which a single pyridine moiety has been removed, and thus allowed for direct comparison of the activity of pentadentate "Py5" versus tetradentate "Py4" ligand complexes [57]. Cyclic voltammograms recorded using a glassy carbon electrode at pH 7 show a plateau-shaped catalytic process with onset potentials ranging from −0.8 V (**10c**) to −1.0 V (**10a-b**) *vs* SHE, preceding direct proton reduction at the glassy carbon electrode. Controlled potential electrolysis (100% faradaic efficiency) carried out at −1.2 V *vs* SHE confirmed the catalytic nature of these pre-waves with moderate TON_{Co} of 60 and 44 achieved after 3 hours for **10a** and **10b**, respectively. Surprisingly, **10c** proved almost entirely inactive for hydrogen evolution during electrolysis, to account for which the authors have suggested competing pathways in its reductive chemistry.

2.3. Cobalt(II)-polypyridyl catalysts displaying ligand-assisted catalytic processes

Ligand-centered redox processes have been characterized in two series of complexes, **7** and **8a-b**, which bear redox-active moieties in the ligand backbone.

Ligand **L7** accommodates Co(II) in a square planar environment in **7**, with two axial chloride ligands completing the coordination sphere [53]. The cyclic voltammogram of **7** in DMF reveals a reversible oxidation process (Co(III/II), +0.43 V *vs* SHE) and three reversible reductive systems at −0.53, −0.78 and −1.13 V *vs* SHE. The first reduction process is assigned to the Co(II/I) couple. The second and third waves, occurring at potentials close to those observed in a voltammogram of the free ligand **L7**, are likely to be ligand-centered. The electrochemistry of **7** is significantly altered in aqueous electrolytes. Aquation of the two axial chloride ligands readily occurs, and the Co(III/II) system is coupled to deprotonation of water ligands in a proton coupled electron transfer (PCET) process. The first cobalt-centered reduction is still observed as a quasi-reversible process occurring at −0.4 V *vs* SHE at all pH values. A pH-dependent catalytic wave assigned to hydrogen evolution is observed at more cathodic potentials, thus it is likely triggered by a ligand-centered reduction process. These results show that ligand-assisted catalytic processes can occur at quite positive potentials in aqueous conditions, and are thus particularly relevant under light-driven conditions.

A similar situation is found with the complexes (**8a-b**) of two pentadentate ligands, **L8a-b**, based on two bipyridine and one pyridine unit [54]. Cyclic voltammetry of the complex **8a**, recorded in acetonitrile, displays three cathodic processes at −1.20 V, −1.79 and −1.94 V *vs* Fc^+/Fc, assigned to the Co(II/I) event and the successive reduction of the two bipyridine units in **L8a**. The Co(III/II) couple appears as a broad event centered at +0.235 V *vs* Fc^+/Fc. The CF_3-substituted complex **8b** shows the expected positive shift of the metal-centered Co(III/II) and Co(II/I) redox couples, by 75 and 61 mV, respectively. More unexpectedly, the ligand based reductions also moved to more positive potentials, by around 80 mV. In both cases, addition of acetic acid triggers the appearance of electrocatalytic waves corresponding to the reduction of protons into hydrogen, with faradaic yields greater than 90%, as confirmed by bulk electrolysis experiments. Two distinct systems, at potentials matching the redox events assigned to ligand-centered reductions, are observed. In the case of **8a**, these peaks are concentration dependent up to 90 mM acetic acid and plateau afterwards, with the second peak giving even higher current densities. For **8b**, the first event shows relatively low current enhancement and levels off quite quickly with the acid concentration. The second event, however, shows much greater current enhancement, although not as high as in the case of **8a**. The authors also recorded cyclic voltammograms in aqueous electrolyte (0.3 M ascorbate buffer, pH 4) on glassy carbon electrodes. Under these conditions, only the Co(II/I) system is observed, the ligand-centered redox processes occurring at potentials where direct proton reduction is readily achieved at the glassy carbon electrode.

No cobalt-centered catalytic process is observed for the complexes **8a-b**, which contrasts with the related pentadentate catalysts **11a-b**, which lack any redox-active ligand. This is likely due to the fact that the introduction of bipyridine moieties in the ligand stabilizes the cobalt center in the reduced state through increased π-back-bonding. This both shifts the

Co(II/I) redox couple to more positive potentials and reduces the nucleophilicity of the Co(I) state. Hence a stronger acid is required for catalysis to be observed. It is likely that a catalytic process could be observed with complexes **8a-b** if TFA was used as a proton source, *i.e.* under conditions similar to those used for assaying the catalytic activity of **3b**, the ligand of which also contains a bipyridine unit, although only binding in a tetradentate manner. Comparing the activity of **3b** and **8a** under similar conditions would also be very interesting in order to verify if the presence of two open or labile coordination sites in *cis* position is beneficial for catalysis.

Despite the large number of electrochemical and electrocatalytic studies available for cobalt(II)-polypyridine complexes, it appears difficult to derive structure-function relationships for this class of compounds, principally because of the large range of experimental conditions used. In particular, data recorded in aqueous solutions are sometimes not exploitable, because the solutions are not properly buffered or because direct hydrogen evolution at the surface of the electrode readily competes with the catalytic process [54].

3. Photocatalytic studies

The light-driven activities of several cobalt(II)-polypyridyl catalysts and of the parent $[Co(bpy)_3]^{2+}$ (**2**) have been evaluated under homogeneous conditions, using a photosensitizer able to harvest light and initiate photoinduced electron transfer, together with a sacrificial electron donor able to regenerate the photosensitizer to its initial state, thus rendering the system catalytic. The structures of the main photosensitizers employed in combination with catalysts **2-12** are presented in Scheme 5, and the photocatalytic performances of these systems are reported in Table 2. Note that unless specifically stated, the formation of cobalt colloids or nanoparticles has been excluded on the basis of the mercury poisoning test or dynamic light scattering measurements in the photocatalytic studies described below.

3.1. Photocatalytic systems based on the parent $[Co(bpy)_3]^{2+}$ complex

Until the late 1970s, most of the work in the area of photocatalytic hydrogen evolving systems relied on the use of $[Ru(bpy)_3]^{2+}$ (**PS1**, Scheme 5) as the photosensitizer in combination with platinum colloids as the heterogeneous hydrogen evolving catalyst [88, 89]. In these systems, cobalt complexes were initially employed as alternative electron relays to methyl-viologen [90-92]. However, blank experiments revealed that hydrogen could also be evolved in the absence of any Pt catalyst [92, 93]. Importantly, these early reports established that in the case of homogeneous cobalt-based hydrogen photoproduction, no electron mediator is required, in contrast to systems based on platinum colloids. In this context, cobalt-bipyridine systems have been extensively studied by Sutin and coworkers [45-50]. Visible light-induced hydrogen evolution was demonstrated as early as 1981, when Co(II) ions and bipyridine were mixed in water at the optimum pH of 5, together with **PS1** and ascorbate in large excess as the sacrificial electron donor [45]. Formation of dihydrobipyridine as a consequence of the reduction of bipyridine was noticed as a side reaction. When bipyridine (**L2a**) was replaced by 4,4′-dimethylbipyridine (**L2b**) in the

catalytic system, a higher quantum yield for hydrogen production was obtained (13% with **L2b** *vs* 2% with **L2a**) [45]. This work has been further improved by using ruthenium tris-dimethylphenanthroline $[Ru(dmphen)_3]^{2+}$(**PS2**, Scheme 5) as the photosensitizer, triethanolamine (TEOA) as the sacrificial electron donor and $[Co(bpy)_3]^{2+}$(**2**) as the catalyst precursor in a 1:1 mixture of acetonitrile and water at pH 8 [48]; under these conditions, a maximum quantum yield of 29% was obtained.

More recently, the chloride salt of **2** was investigated by the group of Bernhard in combination with substituted heteroleptic cyclometallated iridium complexes of the $[Ir(ppy)_2(bpy)]^+$ family (**PS3**, Scheme 5), prepared by a combinatorial chemistry approach [81]. In water acetonitrile mixtures, and in the presence of LiCl and TEOA as the sacrificial electron donor, 16 turnovers based on **2** (TON_{Co}) were achieved by the photocatalytic system, with no significant dependence on the choice of iridium-based photosensitizer (±2 TONs), while the Ru-based **PS1** only allowed for 2 turnovers. Use of **PS2** instead of **PS1** improved the efficiency by a factor of 6, as already observed by Sutin and co-workers [48]. Following this study, **2** has been employed as a reference catalytic system for the evaluation of novel iridium-based photosensitizer structures [82, 94-96], such as charge-neutral amidinate [95] or tricyclometallated derivatives [96]. The reader should note that in all the aforementioned studies, **2** is employed in relatively high excess compared to the iridium-based PS (PS:Cat ratio of 1:20 to 1:50; see table 2), thus accounting for the low TON_{Co} reported in Table 2.

In 2011, Wang, Sun and coworkers reported fully noble metal-free hydrogen evolving photocatalytic systems [83]. Commercially available organic dyes from the xanthene family (**PS6-8**) have been successfully combined with **2** and triethylamine (TEA) as the sacrificial electron donor in an acetonitrile water mixture at pH 10. Under these conditions, the hydrogen evolution efficiency proved to be considerably higher (up to 631 TON_{Co}) than that of similar systems based either on **PS1** or on neutral cobaloximes (**1b**,**c**) as catalysts. Electrostatic attraction between the negatively charged organic dyes and the cationic catalyst has been indicated by UV-vis spectroscopy and proposed as an explanation for the superior performance of these photocatalytic systems.

Finally, a supramolecular strategy, developed by Sakai and coworkers exploited the spontaneous self-assembly of bipyridine-appended cyclometallated iridium photosensitizers in the presence of Co(II) ions, thus generating a $[Co(bpy)_3]^{2+}$ center *in situ*, bearing one, two or three appended photosensitizing units [97]. In the presence of TEOA, these assemblies mediated light-driven hydrogen production in acetonitrile water mixtures with up to 20 TON_{Co}. Multi-component systems tested under the same experimental conditions proved to be half as efficient, demonstrating the importance of the supramolecular design.

3.2. Photocatalytic systems based on cobalt(II)-polypyridyl catalysts

Since the first report in 2010 by Chang and coworkers on the cobalt(II)-polypyridyl electrocatalyst **3b** [52], a great deal of effort has been devoted to the design of original polypyridyl ligands and the evaluation of their cobalt complexes in light-driven hydrogen evolution. In contrast with the cobaloximes, no supramolecular or covalent photosensitizer-

catalyst assembly has to date been reported for cobalt(II)-polypyridyl catalysts, to the best of our knowledge.

In 2012, Lau and coworkers reported the hydrogen evolution activity of the bis-aqua catalyst **5a** in combination with either **PS3** or the fluorinated derivative **PS4**, in presence of TEOA as sacrificial electron donor and *p*-cyanoanilinium tetrafluoroborate as proton source [84]. Under optimized conditions (**PS4**:Cat ratio of 1:20), 58 TON_{Co} have been measured in a 95:5 acetonitrile water mixture. After 20 hours, addition of extra photosensitizer could reinitiate catalysis. In contrast, catalyst **2** and the related $[Co(bpy)_2(OH_2)_2]^{2+}$ display much lower TONs, and catalysis could not be reinitiated by addition of PS. It should be noted that this study is the only one of the polypyridyl series reported under organic conditions and producing a clear comparison with the parent catalyst **2**. In addition, catalyst **5a** was recently reevaluated by Long, Chang, Castellano and coworkers under fully aqueous conditions (**PS1**, ascorbic acid as sacrificial electron donor at pH 5.5) and performed up to 200 TON_{Co} which ranks it among the less active polypyridyl catalysts of the tested series (from 150 to 1850 TON_{Co} for catalysts **3a-6** and **10a-11c** tested under identical conditions; see section 3.3 below for more detailed comparison) [57].

Hydrogen evolving photocatalytic activity of cobalt(II)-polypyridyl catalysts in fully aqueous medium was first reported in early 2013 with catalysts **11a-c** [59] and **3a** [85]. Long, Chang and coworkers have demonstrated that the family of complexes **11a-c**, previously described as highly efficient electrocatalysts in neutral water [58], were also active under visible light-driven conditions in the presence of **PS1** and ascorbate in aqueous phosphate buffer at pH 7. Catalyst **11a** exhibited the highest performance in the series, in good agreement with its low overpotential for electrocatalytic hydrogen evolution [58]. The authors established that photosensitizer decomposition was the primary reason for the cease of activity after 8 hours of photolysis. Hydrogen evolution was also demonstrated in combination with a semiconductor nanowire photosensitizer, which is, however, out of the scope of this review [59]. At the same time, Hamm, Alberto and coworkers have prepared and tested the dibromo complex **3a** in combination with the rhenium-based photosensitizer **PS5** in ascorbate buffer at pH 4.1 [85]. Up to 9000 TON_{Co} were obtained, however at very low concentration of catalyst (0.1 μM) and extremely high PS:Cat ratio (5000:1). The long-term stability of the system has been studied using a higher concentration of catalyst (0.5 mM) producing 0.52 mmol hydrogen (104 TON_{Co}) over 120 hours. At the end of the photocatalysis experiments, LC-MS analysis showed the presence of both catalyst and **PS5** (≥ 90%), demonstrating their stability. Two new pentadentate ligands and their cobalt catalysts have also been reported by the same authors [86]. The first, **L9**, displays a "Bpy_2Py" coordination sphere whereas the second ligand, **L12a**, relies on a "Py_5" scaffold closely related to **L11b** [58, 59]. From a series of first-row transition metal complexes (Mn(II), Fe(II), Co(II), Ni(II), Cu(II), Zn(II)) evaluated as water reduction catalysts, the cobalt complexes alone displayed some hydrogen evolution activity. TON_{Co} as high as 1380 for **9** and 1180 for **11a** were recorded, using 100 equivalents of **PS5** in aqueous solution of ascorbate (pH 4.1). Loss of catalytic activity under these conditions was assigned to competitive back electron transfer from the reduced photosensitizer PS^- to dehydroascorbic acid (DHA), formed by oxidation of ascorbic acid [85, 86]. Such self-inhibition by the

oxidized form of the sacrificial electron donor, accumulated during the course of the catalysis, has been also identified in other studies as a limitation of the ascorbate-based systems [56, 57]. This drawback has been recently elegantly circumvented by using the reversible ascorbate system as an electron relay between the photosensitizer (**PS1** or **PS5**) and a tertiary phosphine-based irreversible electron donor (tris(2-carboxyethyl)phosphine, TCEP) [87]. Higher hydrogen evolution rates and total amounts of hydrogen could thus be obtained. This work from Alberto and coworkers opens new perspectives for the optimization of light-driven hydrogen evolution under fully aqueous medium.

Two other examples of "Bpy_2Py"-type ligands, **L8a-b**, were later reported by Chang, Long, Castellano and coworkers [54]. In good agreement with the electrocatalytic studies, catalyst **8b**, bearing electron-withdrawing CF_3 groups, displayed a lower light-driven activity than **8a** (1630 TON_{Co} with Φ 3.6% versus 1390 TON_{Co} with Φ 2.7%, respectively). The authors demonstrated that under the reported experimental conditions, photocatalytic activity was solely limited by photosensitizer stability.

In 2014, Thummel and coworkers tested complex **7**, a hydrogen evolving electrocatalyst active under neutral aqueous conditions, in combination with the classical **PS1**-ascorbate system, and up to 333 TON_{Co} were measured during the course of a three hour experiment under LED irradiation [53]. Meanwhile, Scandola and coworkers have evaluated catalyst **12b** in presence of **PS1** in aqueous ascorbate buffered solution (pH 4) [56]. Under visible light irradiation, 187 TON_{Co} were achieved in one hour. The authors have shown that TON_{Co} values were insensitive to catalyst concentration, in contrast with what is usually observed for the other reported polypyridyl cobalt-based systems.

Finally, Long, Chang, Castellano and coworkers have undertaken the benchmarking of 10 distinct catalysts (**3-6**, **10-11**) under identical conditions (2×10^{-5} M catalyst, 3.3×10^{-4} M **PS1** in 0.3 M aqueous ascorbate buffer; irradiation at 452 nm) in order to provide comprehensive findings and guidelines for the design of optimized systems [57]. A systematic adjustment of the pH has been made for each individual catalyst in order to take into account the variations in relative basicity of the Co(I) intermediate likely to be protonated during the cobalt-based catalytic cycle (see section 2.1 for mechanistic details). In this study, new ligands (**L4a,b** and **L10a-c**) were synthesized to more accurately evaluate parameters such as electronic effects of substituents (**L4** series) and the tetradentate versus pentadentate nature of the ligands (**L10** series). The results from this study are highlighted in the next section.

3.3. Structure-photocatalytic activity relationships

Specific catalyst structure-photocatalytic activity relationships arise from the reported studies on cobalt(II)-polypyridyl photocatalytic systems. Although a straightforward comparison of the activities reported in Table 2 cannot be made for all the systems due to differences in the experimental conditions employed, a strong influence of the ligand structure and coordination sphere of the cobalt center is observed. A series of structural relationships identified in the cobalt-polypyridyl catalyst series are listed below and their influence on the photocatalytic activity tentatively assigned; as more than one relationship

often exists between the catalysts considered, the discussion necessarily overlaps at some points.

Tris-bipyridine vs polypyridyl—Going from the simple bipyridine ligand **L2a** to polypyridine structures with higher denticities is proposed to confer higher stability to the cobalt complex in its reduced states by virtue of the chelate effect, and as a consequence improve the efficiency of the catalytic system. The parent complex **2** is known to be active upon the loss of one bipyridine ligand [49], whereas penta- and tetradentate ligands allow one and two coordination sites, respectively, to remain vacant on the cobalt center for catalysis to occur *via* formation of a cobalt hydride species (see section 2.1). There is only one example in the literature where **2** and a cobalt(II)-polypyridyl catalyst are compared under similar conditions: Lau and coworkers have shown that the tetradentate quaterpyridine catalyst **5a** displays much higher TONs than **2** and the related $[Co(bpy)_2(OH_2)_2]^{2+}$; moreover, whereas catalysis could be reinitiated by addition of photosensitizer in case of **5a**, full decomposition of the catalyst was observed with **2** and $[Co(bpy)_2(OH_2)_2]^{2+}$ [84]. This result can be correlated with the formation of dihydrobipyridine by reduction of the bipyridine ligand observed in the early works from Sutin and coworkers [45]. It should be noted, however, that the relative arrangement of the two aqua ligands differs between these complexes, *trans* in **5a** versus presumably *cis* in $[Co(bpy)_2(OH_2)_2]^{2+}$, which could also influence the reactivity (see below). In contrast, the stability of catalyst **3a** has been assessed by LC-MS analysis of the photocatalytic system, and it was established that 96.5% of **3a** is still present after 120 hours of irradiation [85]. Similarly, HPLC control experiments established that 90% of **4a** remained intact at the end of the photocatalytic test (~2 hours) [57]. Thus, no reduction of the bipyridine moieties occurred on the tetradentate bpy-based ligands **L3a** and **L4a**.

Bipyridine-based vs pyridine-based ligands—Two main consequences stem from the presence of a bipyridine moiety in the ligand structure as compared with single pyridine moieties: (i) more sterically constrained geometries around the cobalt center are obtained and (ii) ligand-centered redox processes can occur (see section 2.3). The former effect has been put forward by Hamm, Alberto and coworkers to explain the higher activity of **9** compared to **12a** [86]. Complex **9** indeed displays a much more strongly distorted octahedral structure compared to that of **12a**, and was shown to catalyze hydrogen evolution at faster rate. However, these two series of complexes also differ due to more subtle effects linked to the orientation of the pyridyl rings of the ligand within the complexes: while π-π overlap between the pyridyl rings in the **11-12** series is possible, in the series **8-9**, the positioning of the four rings in the equatorial plane prevents it. The photocatalytic activity of pentadentate catalysts **8a-b**, bearing a redox-active bipyridine, clearly outperformed catalysts **11**, relying on a "Py_5" structure [54]. The superiority of bipyridine-based structures is, however, less marked in the tetradentate series, where "$BpyPy_2$" ligands **L3a-L4b** have been compared to "Py4" ligands **L10a-c** under similar conditions [57]. Catalyst **4a** displayed the highest activity with 1850 TONs achieved in 14 hours, however it is closely followed by **10a** (1550 TONs). Electronic and steric effects of the substituents also come into play when considering the other complexes of the two series, **3a'** (950 TONs), **3b** (1025 TONs), **4b** (400 TONs), **10b** (250 TONs) and **10c** (225 TONs). The contribution of ligand-centered

redox processes to hydrogen evolution activity is thus difficult to properly demonstrate under light-driven conditions.

Pentadentate vs tetradentate ligands—During the course of their benchmarking of cobalt(II) catalysts, Long, Chang, Castellano and coworkers have designed three new tetradentate ligands **L10a-c**, based on the parent pentadentate structure **L11b**, but with one fewer pyridine moiety [57]. These two series of ligands thus allow for an accurate comparison of the influence of the ligand denticity on the hydrogen evolution activity of the corresponding cobalt catalysts. It was established that tetradentate ligands led to significantly more active catalysts (1550 TON_{Co} for **10a** versus 300 TON_{Co} for **11b** under the same experimental conditions), but this effect cannot be generalized since more sterically hindered catalysts **10b** and **10c** display activities 6 to 8 times lower than **10a**, reflecting the trend observed in the course of electrochemical studies [57]. The structures of catalysts **3a** [85] and **9** [86] also only differ by the denticity of their ligands, tetradentate for **L3a** versus pentadentate for **L9**. Under similar photocatalytic conditions (5 μM in catalyst, 100:1 **PS5**:Cat ratio, ascorbate buffer pH 4.1), **3a** proved to be slightly superior, with ~2000 TONs achieved *vs* 1380 TONs for **9**. From this analysis, it is not possible to demonstrate a clear advantage of tetradentate ligands over pentadentate ligands. It should also be mentioned that a closely related pentadentate system [80] undergoes decoordination of one pyridine arm in the course of catalysis (described in more detail later in the discussion), thus leading to a pseudo-tetradentate system.

Cis vs trans open coordination sites—Catalysts bearing tetradentate bipyridine-based ligands (**3-7** in Scheme 2) can be distinguished by the *cis*/*trans* stereochemistry of the two labile positions on the cobalt complex. The *cis* stereochemistry in complexes **3a-4b** is controlled by ligands bearing one bipyridine moiety plus two appended pyridines, whereas *trans* complexes **5a-7** rely on two diimine moieties (bipyridine or phenanthroline) in their coordination sphere. In order to establish the influence of the *cis*/*trans* geometry on the light-driven hydrogen evolution activity, the groups of Castellano, Long and Chang have benchmarked catalysts **3a-6** (initially described either in their groups or in other research groups) under identical experimental conditions. This allowed them to establish that catalysts with *cis* open coordination sites significantly outperform those with *trans* sites (up to 1850 TON_{Co} for **4a** versus 200 and 150 TON_{Co} for **5a** and **6**, respectively) [57].

Nature of the labile monodentate ligand(s) on the cobalt center—Subtle variations of the monodentate ligand(s) that complete the coordination sphere of the catalyst are observed. They can be monoanions, such as Cl^-, Br^-, OTf^-, or solvent molecules (CH_3CN; H_2O), thus leading to either neutral, monocationic or dicationic cobalt catalysts. The nature of these ligands is generally dictated by the choice of the cobalt salts used for the metallation reaction and also by some solubility issues in water. Although ligand **L3a** has, for instance, been employed by two independent groups, with different labile ligands on the cobalt center, the dicationic hexacoordinated bis-acetonitrile complex **3a'** [57] and the monocationic pentacoordinated bromo complex **3a** [85], a direct comparison of their relative efficiencies is precluded as very different conditions for their evaluation have been used (**PS1** for **3a'** versus **PS5** for **3a**, in different PS:Cat ratios). Chloride substitution by water

has been electrochemically observed for **7** under aqueous conditions. Anation by the acetate anion occurred during the course of the electrocatalytic study on catalysts **11a-b**, shifting the redox potential of the Co(II/I) couple toward more cathodic potentials. If such a monodentate ligand remains coordinated in the Co(I) state, it may also influence the protonation steps. These labile positions are thus highly sensitive to their environment.

During the course of photocatalysis, formation of a cobalt hydride intermediate (see section 2.1) is expected to occur with displacement of one monodentate ligand; at the end of the hydrogen evolution catalytic cycle, the cobalt center will be recovered either in a solvated form or coordinated by a new monodentate ligand, depending on the anion present in the medium. The situation could be a little bit trickier for catalysts based on pentadentate ligands. It has been established on a closely related pentadentate aminopyridinic system that formation of Co(III)–H occurs *via* decoordination of one pyridine arm of the ligand, rather than by removal of the chloride monodentate ligand from the cobalt center [80]. Indeed, four catalysts differing only by the nature of the monodentate ligand (Cl^-, NO_3^-, OTf^-, H_2O) displayed very different activities, the chloride derivative being the most active and the nitrate five times less active. Furthermore, activity was enhanced in 0.3 M NaCl solution, and decoordination of one pyridine arm was established by NMR under acidic conditions. This highly counter-intuitive result emphasizes the necessity to correctly establish the cobalt-center hydrogen evolution mechanism in order to optimize the photocatalytic activity of such systems. The influence of the so-called labile positions on the cobalt center deserves to be more systematically studied in the future.

Ligand substituent electronic effects—The first pentadentate family of ligands **L11a-c** studied by Chang and coworkers consisted of three structures differing only in the central pyridine *para*-substituent: electron-withdrawing -CF_3 group in **L11a**, -H in **L11b** and electron-donating -NMe_2 group in **L11c**. In excellent agreement with the electrocatalytic studies, catalyst **11a** proved to be the most efficient of the series, producing twice the amount of hydrogen of **11c** after 8 hours of visible light irradiation (LED 452 nm) [59]. On the basis of these results, the same authors designed two new sets of ligands **4a**,**b** [57] and **8a**,**b** [54], **4b** and **8b** bearing CF_3 substituents on the pyridine moieties. However, the latter displayed lower activities than the parent H-substituted **3a** and **8a** under both electro- and photocatalytic conditions [54, 57]. Of note is the fact that these two series of complexes possess redox-active bipyridine moieties, in contrast to **11a-c**, with a ligand-assisted catalytic process being clearly established for **8a-b** (see section 2.3). Substitution of CF_3 on the bipyridine rather than on the pyridine moiety would therefore be interesting to investigate, in order to electronically modulate the ligand-assisted process.

Another type of substituent effect is addressed in the **3a'**,**b-4a** series of catalysts, the ligand structures of which vary only in the substitution on the central quaternary carbon (Me, OH or OMe). The recent comparative study by Long, Chang, Castellano and coworkers established that the presence of the methyl substituent confers a greatly enhanced catalytic activity in comparison with the OH or OMe derivatives (1850 TON_{Co} for **4a** *vs* 950 TON_{Co} for **3a'** and 1025 TON_{Co} for **3b**) [57]. However, such a variation in activity is difficult to rationalize on the basis of simple electronic effects. Modification of the substitution of a

bridging carbon is also encountered in the series **10a-c**. The increase in steric hindrance, observed in going from **10a** (bridging CH_2) to **10c** (bridging $C(Me)_2$), drastically influences the light-driven activity of these catalysts, with **10a** being one of the more efficient in the field while **10b** and **10c** display low activities [57]. This effect is also observed in the electrocatalytic studies.

3.4. Mechanistic considerations

One important development with the cobalt(II)-polypyridyl catalysts has been the ability to perform photocatalytic tests under fully aqueous conditions, thanks to the increased stability of the cobalt coordination sphere towards both hydrolysis and reductive conditions. This has allowed the commonly used amine sacrificial electron donors (TEA, TEOA), which require working at basic pH, to be avoided. The ascorbic acid/ascorbate couple, active at the optimal pH of 4-5, can be employed instead, allowing conditions for the photocatalytic tests to better match those favoring hydrogen evolution. It should be noted, however, that the pH of the medium is only precisely defined in fully aqueous conditions; strong uncertainty exists for both the pH value and pKa of the sacrificial electron donor when pure organic or mixed organic/aqueous solutions are employed.

The photosensitizer-based mechanisms are presented in Figure 2. In contrast with electrocatalysis performed under the control of a potentiostat, the reductive power of the medium cannot be adjusted on demand under light-driven conditions, but is fixed by the redox levels of the photosensitizer. In addition, the concentration of reducing equivalents is controlled by sequential monoelectronic processes induced by photon absorption and thus limited by the photon flux. The reductive species for the Co(II) center can be either PS* *via* an oxidative quenching pathway (Figure 2, right) or PS^- *via* a reductive quenching mechanism (Figure 2, left). Mechanistic studies are therefore mostly focused on the elucidation of the photosensitizer-based processes, through the use of time-resolved spectroscopic measurements that allow observation of signatures associated with the intermediate forms of the photosensitizer.

When $[Co(bpy)_3]^{2+}$ (**2**) is used as the catalyst in a photochemical hydrogen evolving system, it can be reduced to $[Co(I)(bpy)_3]^+$ either by PS* (**PS1*** or **PS2***) *via* the oxidative quenching process or by PS^-, generated from the reductive quenching of PS* by D [50]. The work of Sutin and coworkers established that the reductive quenching process takes place when ascorbate is used as sacrificial electron donor [45, 46, 50], whereas the oxidative quenching mechanism is at work with TEOA [48, 50]. Generation of cobalt(I) complexes from **2** under irradiation is evidenced by the blue color of the solution, and dissociation of bipyridine ligands from $[Co(I)(bpy)_3]^+$ has been observed under catalytically relevant conditions [49]. In fact, the hydride complex $[Co(bpy)_2(OH_2)H]^{2+}$, independently prepared by pulse radiolysis of aqueous $CoSO_4$-bipyridine mixtures in the presence of radical scavengers [47], is likely the key catalytic intermediate during hydrogen photogeneration from aqueous solutions [48, 50]. It should also be noted that the major cobalt(II) complexes formed in solution are the mono and bis-bipyridine $[Co(bpy)_n]^{2+}$ (n = 1 and 2) species if the catalytic mixture is prepared by mixing a Co(II) salt with the diimine ligand (**L2a** or **L2b**; Co(II):L = 5:1, see Table 2) [45].

Reductive quenching of **PS1*** by ascorbate is also recognized as the predominant process in most of the photocatalytic systems based on polypyridyl catalysts [57]. **PS1*** is, for instance, not quenched by catalyst **8a** at the concentrations used in the photocatalytic experiments, whereas a reductive quenching constant of 2.6×10^7 $M^{-1}\cdot s^{-1}$ has been measured with ascorbate at pH 4 [54]. Oxidative quenching of **PS1*** by catalyst **4a** has been calculated to be thermodynamically disfavored from the potentials of the two redox couples [57]. In contrast, both oxidative and reductive processes are allowed for the photocatalytic system based on **12b**, **PS1** and ascorbate; bimolecular rate constants of 3.1×10^8 $M^{-1}\cdot s^{-1}$ and 1.0×10^7 $M^{-1}\cdot s^{-1}$ for **12b** and ascorbate, respectively, have been obtained from steady-state quenching experiments [56]. However, despite a difference of one order of magnitude between these two constants, the reductive quenching process is dominant under the employed photocatalytic conditions (0.1 M in ascorbate versus 10-100 μM in **12b**). Formation of reduced $[Ru(bpy)_3]^+$ has moreover been confirmed by laser flash photolysis experiments, and subsequent electron transfer to **12b** occurred with a bimolecular rate constant estimated to be 5.7×10^9 $M^{-1}\cdot s^{-1}$ [56]. Such high values, close to the diffusion limit, have also been measured for closely related systems based on aminopyridyl ligands [98, 99]. Fast electron transfer from PS^- to the catalyst is required to optimize the photocatalytic performances of a system by limiting decomposition of the reduced photosensitizer PS^-.

Nevertheless, these photophysical studies generally only address the first electron transfer process occurring in the catalytic cycle, that is the initial reduction of a Co(II) complex to a Co(I) state (Figure 1). A second photoinduced electron transfer is required to produce hydrogen, either to reduce a Co(III)–H species (ECEC pathway, Figure 1), for a second reduction of the Co(I) intermediate (EECC pathways, Figure 1) or, alternatively, to regenerate the initial Co(II) state of the catalyst (ECCE pathway, Figure 1). Very little is known about the cobalt-centered mechanism taking place under light-driven conditions. The hydrogen evolution rate is, in many examples [59, 85, 100], reported to be first-order with catalyst concentration for experiments performed at relatively low catalytic concentrations, which reflects the fact that the rate determining step is the electron transfer from the photosensitizer to the catalyst, the hydrogen evolution rate being generally proportional to the photon flux. At the same time, such a dependency likely excludes homolytic mechanisms that are strongly disfavored at low catalyst concentration. Such conditions, however, are not relevant from a practical point of view since very low amounts of hydrogen are produced (see Table 2), and substantial production of hydrogen is generally obtained at higher catalyst concentrations (see Table 2 and, for instance, reference [85]). The Co(III)–H based ECCE pathway (Figure 1) requires strong acids to operate and is thus very unlikely to take place under the reported photocatalytic conditions; pathways involving a Co(II)–H species are therefore favored. Thermodynamics indicates that the reductive strength of $[Ru(bpy)_3]^+$(−1.26 V *vs* NHE) is high enough to further reduce the Co(I) state of catalysts such as **8a**,**b** [54], thus allowing the ligand-assisted EECC pathway, characterized in the electrocatalytic studies, to also operate under photocatalytic conditions. Of note are the studies from Long, Chang and coworkers where both electrocatalytic and photocatalytic experiments were undertaken in pH 7 aqueous phosphate buffer for catalysts **11a-c** [58, 59] and in pH 4 ascorbate buffer for **4a**,**b**. In both cases, the redox potential of $[Ru(bpy)_3]^+$ is more cathodic than the onset potential of the electrocatalytic wave which demonstrates the

ability of **PS1** to drive hydrogen production under visible light irradiation. In general however, comparison of the electrocatalytic and photocatalytic studies is precluded as they are performed under too dissimilar experimental conditions. It has also been recently highlighted that electrocatalytic and photocatalytic processes may proceed through distinct mechanisms, especially if the former involves two successive electron transfers [101]. In a very recent study published during the course of preparing this review, Hamm and coworkers addressed this mechanistic issue by performing spectroscopic studies combined with *in-situ* time-resolved hydrogen detection [102]; a three-component system based on **PS5**, **3a** and TEOA was shown to evolve hydrogen *via* the heterolytic ECEC pathway (Figure 1), an identical mechanism to that previously established for cobaloximes.

4. Conclusion and outlook

The electro- and photocatalytic systems based on hydrogen evolving molecular cobalt(II)–polypyridyl catalysts are distinguished from the previous cobaloxime and $[Co(bpy)_3]^{2+}$ based catalysts by the robustness of the polypyridyl coordination sphere toward either reduction, hydrolysis or ligand exchange under reductive conditions. Thanks to this property, light-driven hydrogen evolution has been successfully achieved under fully aqueous conditions using ascorbate as the sacrificial electron donor. Obviously, working under aqueous acidic conditions is beneficial for the cobalt-centered mechanisms and represents an important development in the field. It should nevertheless be emphasized that combined experimental-theoretical mechanistic studies are still needed to fully understand the catalytic mechanism, with a special focus on the beneficial role played by redox-active centers often present in the ligand structure, such as the bipyridine moiety.

Thanks to the wide variety of polypyridyl ligands evaluated during the last four years, structure-activity relationships were tentatively established in order to shed light on some specific trends for the future design of better performing catalytic systems. First, the relatively high sensitivity of the light-driven hydrogen evolving activity to very subtle variations on the ligand backbone should be noted from these studies. Although catalysts based on tetradentate ligands were reported to be superior to pentadentate ones, no obvious advantage could be established here, as substitution on the ligand backbone also strongly influences the activity, without clear rationale. Only the presence of two *cis* open coordination sites in the tetradentate series can be recognized as beneficial for the catalytic activity. We nonetheless would like to draw the reader's attention to the fact that a straightforward comparison of the reported numerical values such as TONs can be misleading in comparing different catalysts. TON values are indeed highly dependent on the photocatalytic experimental conditions that, in most cases, drastically vary from one study to another. High TON_{Co} can be reached at low catalyst concentration but to the detriment of the long term stability and of the quantity of hydrogen produced. As a consequence, quantum yield together with long-term stability should be the two parameters to more systematically consider in the future.

These studies clearly open new perspectives in the field of light-driven hydrogen evolution by molecular cobalt catalysts. Up to now, the prototype ruthenium trisbipyridine was the main photosensitizer used in aqueous media, but new light-harvesting units can now be

considered to improve both the activity and the sustainability of these photocatalytic systems. In addition, the phosphine (sacrificial electron donor) ascorbate (electron relay) combination developed by Alberto and coworkers [87] should be systematically evaluated to overcome the limitations imposed by the dehydroascorbate deactivation pathway.

Acknowledgements

This work was supported by the COST Action CM1202 PERSPECT-H_2O, the French National Research Agency (Labex program, ARCANE, ANR-11-LABX-0003-01), the FCH Joint Undertaking (ArtipHyction Project, Grant Agreement n.303435), the European Research Council under the European Union's Seventh Framework Programme (FP/2007-2013)/ERC Grant Agreement n.306398 and the Life Science Division of CEA (2011 DSV-Energy program).

References

[1]. Armaroli N, Balzani V. Chemsuschem. 2011; 4:21–36. [PubMed: 21226208]

[2]. Hambourger M, Moore GF, Kramer DM, Gust D, Moore AL, Moore TA. Chem. Soc. Rev. 2009; 38:25–35. [PubMed: 19088962]

[3]. Ghirardi ML, Zhang JP, Lee JW, Flynn T, Seibert M, Greenbaum E, Melis A. Trends Biotechnol. 2000; 18:506–511. [PubMed: 11102662]

[4]. Stripp ST, Happe T. Dalton Trans. 2009:9960–9969. [PubMed: 19904421]

[5]. Andreiadis ES, Chavarot-Kerlidou M, Fontecave M, Artero V. Photochem. Photobiol. 2011; 87:946–964. [PubMed: 21740444]

[6]. Joya KS, Joya YF, Ocakoglu K, van de Krol R. Angew. Chem. Int. Ed. 2013; 52:10426–10437.

[7]. Berardi S, Drouet S, Francas L, Gimbert-Surinach C, Guttentag M, Richmond C, Stoll T, Llobet A. Chem. Soc. Rev. 2014; 43:7501–7519. [PubMed: 24473472]

[8]. Song W, Chen Z, Brennaman MK, Concepcion JJ, Patrocinio AOT, Iha NYM, Meyer TJ. Pure Appl. Chem. 2011; 83:749–768.

[9]. Gust D, Moore TA, Moore AL. Acc. Chem. Res. 2009; 42:1890–1898. [PubMed: 19902921]

[10]. Magnuson A, Anderlund M, Johansson O, Lindblad P, Lomoth R, Polivka T, Ott S, Stensjö K, Styring S, Sundström V, Hammarström L. Acc. Chem. Res. 2009; 42:1899–1909. [PubMed: 19757805]

[11]. Reisner E. Eur. J. Inorg. Chem. 2011; 2011:1005–1016.

[12]. Krassen H, Ott S, Heberle J. Phys. Chem. Chem. Phys. 2011; 13:47–57. [PubMed: 21103567]

[13]. Wang F, Wang W-G, Wang H-Y, Si G, Tung C-H, Wu L-Z. ACS Catalysis. 2012; 2:407–416.

[14]. Woolerton TW, Sheard S, Chaudhary YS, Armstrong FA. Energy Environ. Sci. 2012; 5:7470–7490.

[15]. Chavarot-Kerlidou, M.; Chenevier, P.; Artero, V. Bio–Organometallic Systems for the Hydrogen Economy: Engineering of Electrode Materials and Light–Driven Devices. In: Jaouen, Gérard; Salmain, Michèle, editors. Bioorganometallic Chemistry: Applications in Drug Discovery, Biocatalysis, and Imaging. Wiley–VCH Verlag GmbH & Co. KGaA, Boschstr. 12, 69469; Weinheim, Germany: 2015. In press

[16]. Losse S, Vos JG, Rau S. Coord. Chem. Rev. 2010; 254:2492–2504.

[17]. Artero V, Chavarot-Kerlidou M, Fontecave M. Angew. Chem. Int. Ed. 2011; 50:7238–7266.

[18]. Razavet M, Artero V, Fontecave M. Inorg. Chem. 2005; 44:4786–4795. [PubMed: 15962987]

[19]. Hu XL, Cossairt BM, Brunschwig BS, Lewis NS, Peters JC. Chem. Commun. 2005:4723–4725.

[20]. Baffert C, Artero V, Fontecave M. Inorg. Chem. 2007; 46:1817–1824. [PubMed: 17269760]

[21]. Hu X, Brunschwig BS, Peters JC. J. Am. Chem. Soc. 2007; 129:8988–8998. [PubMed: 17602556]

[22]. Du PW, Knowles K, Eisenberg R. J. Am. Chem. Soc. 2008; 130:12576–12577. [PubMed: 18759395]

[23]. Du PW, Schneider J, Luo GG, Brennessel WW, Eisenberg R. Inorg. Chem. 2009; 48:8646–8646.

[24]. Lazarides T, McCormick T, Du PW, Luo GG, Lindley B, Eisenberg R. J. Am. Chem. Soc. 2009; 131:9192–9194. [PubMed: 19566094]

[25]. McCormick TM, Calitree BD, Orchard A, Kraut ND, Bright FV, Detty MR, Eisenberg R. J. Am. Chem. Soc. 2010; 132:15480–15483. [PubMed: 20945839]

[26]. Probst B, Kolano C, Hamm P, Alberto R. Inorg. Chem. 2009; 48:1836–1843. [PubMed: 19235947]

[27]. Probst B, Rodenberg A, Guttentag M, Hamm P, Alberto R. Inorg. Chem. 2010; 49:6453–6460. [PubMed: 20553017]

[28]. Zhang P, Wang M, Dong J, Li X, Wang F, Wu L, Sun L. J. Phys. Chem. C. 2010; 114:15868–15874.

[29]. Wang X, Goeb S.b. Ji Z, Pogulaichenko NA, Castellano FN. Inorg. Chem. 2011; 50:705–707. [PubMed: 21204549]

[30]. Khnayzer RS, McCusker CE, Olaiya BS, Castellano FN. J. Am. Chem. Soc. 2013; 135:14068–14070. [PubMed: 24028290]

[31]. Fihri A, Artero V, Razavet M, Baffert C, Leibl W, Fontecave M. Angew. Chem. Int. Ed. 2008; 47:564–567.

[32]. Fihri A, Artero V, Pereira A, Fontecave M. Dalton Trans. 2008:5567–5569. [PubMed: 18854893]

[33]. Zhang P, Wang M, Li C, Li X, Dong J, Sun L. Chem. Commun. 2010; 46:8806–8809.

[34]. Cropek DM, Metz A, Muller AM, Gray HB, Horne T, Horton DC, Poluektov O, Tiede DM, Weber RT, Jarrett WL, Phillips JD, Holder AA. Dalton Trans. 2012; 41:13060–13073. [PubMed: 23001132]

[35]. Veldkamp BS, Han W-S, Dyar SM, Eaton SW, Ratner MA, Wasielewski MR. Energy Environ. Sci. 2013; 6:1917–1928.

[36]. Bartelmess J, Weare WW, Sommer RD. Dalton Trans. 2013; 42:14883–14891. [PubMed: 23989263]

[37]. Peuntinger K, Lazarides T, Dafnomili D, Charalambidis G, Landrou G, Kahnt A, Sabatini RP, McCamant DW, Gryko DT, Coutsolelos AG, Guldi DM. The Journal of Physical Chemistry C. 2012; 117:1647–1655.

[38]. Natali M, Argazzi R, Chiorboli C, Iengo E, Scandola F. Chemistry – A European Journal. 2013; 19:9261–9271.

[39]. Manton JC, Long C, Vos JG, Pryce MT. Dalton Trans. 2014; 43:3576–3583. [PubMed: 24399269]

[40]. Jacques P-A, Artero V, Pécaut J, Fontecave M. Proc. Natl. Acad. Sci. U.S.A. 2009; 106:20627–20632. [PubMed: 19948953]

[41]. Probst B, Guttentag M, Rodenberg A, Hamm P, Alberto R. Inorg. Chem. 2011; 50:3404–3412. [PubMed: 21366324]

[42]. Guttentag M, Rodenberg A, Kopelent R, Probst B, Buchwalder C, Brandstätter M, Hamm P, Alberto R. Eur. J. Inorg. Chem. 2012; 2012:59–64.

[43]. Zhang P, Jacques P-A, Chavarot-Kerlidou M, Wang M, Sun L, Fontecave M, Artero V. Inorg. Chem. 2012; 51:2115–2120. [PubMed: 22313315]

[44]. Andreiadis ES, Jacques P-A, Tran PD, Leyris A, Chavarot-Kerlidou M, Jousselme B, Matheron M, Pécaut J, Palacin S, Fontecave M, Artero V. Nat Chem. 2013; 5:48–53. [PubMed: 23247177]

[45]. Krishnan CV, Sutin N. J. Am. Chem. Soc. 1981; 103:2141–2142.

[46]. Krishnan CV, Creutz C, Mahajan D, Schwarz HA, Sutin N. Isr. J. Chem. 1982; 22:98–106.

[47]. Creutz C, Schwarz HA, Sutin N. J. Am. Chem. Soc. 1984; 106:3036–3037.

[48]. Krishnan CV, Brunschwig BS, Creutz C, Sutin N. J. Am. Chem. Soc. 1985; 107:2005–2015.

[49]. Schwarz HA, Creutz C, Sutin N. Inorg. Chem. 1985; 24:433–439.

[50]. Creutz C, Sutin N. Coord. Chem. Rev. 1985; 64:321–341.

[51]. Artero V, Saveant J-M. Energy Environ. Sci. 2014; 7:3808–3814. [PubMed: 26269710]

[52]. Bigi JP, Hanna TE, Harman WH, Chang A, Chang CJ. Chem. Commun. 2010; 46:958–960.

[53]. Tong L, Zong R, Thummel RP. J. Am. Chem. Soc. 2014; 136:4881–4884. [PubMed: 24635104]

[54]. Nippe M, Khnayzer RS, Panetier JA, Zee DZ, Olaiya BS, Head-Gordon M, Chang CJ, Castellano FN, Long JR. Chemical Science. 2013; 4:3934–3945.

[55]. King AE, Surendranath Y, Piro NA, Bigi JP, Long JR, Chang CJ. Chemical Science. 2013; 4:1578–1587.

[56]. Deponti E, Luisa A, Natali M, Iengo E, Scandola F. Dalton Trans. 2014; 43:16345–16353. [PubMed: 25237910]

[57]. Khnayzer RS, Thoi VS, Nippe M, King AE, Jurss JW, El Roz KA, Long JR, Chang CJ, Castellano FN. Energy Environ. Sci. 2014; 7:1477–1488.

[58]. Sun Y, Bigi JP, Piro NA, Tang ML, Long JR, Chang CJ. J. Am. Chem. Soc. 2011; 133:9212–9215. [PubMed: 21612276]

[59]. Sun Y, Sun J, Long JR, Yang P, Chang CJ. Chemical Science. 2013; 4:118–124.

[60]. Kölle U, Ohst S. Inorg. Chem. 1986; 25:2689–2694.

[61]. Wiedner ES, Appel AM, DuBois DL, Bullock RM. Inorg. Chem. 2013; 52:14391–14403. [PubMed: 24261463]

[62]. Muckerman JT, Fujita E. Chem Commun. 2011:12456–12458.

[63]. Solis BH, Hammes-Schiffer S. Inorg. Chem. 2011; 50:11252–11262. [PubMed: 21942543]

[64]. Solis BH, Yu Y, Hammes-Schiffer S. Inorg. Chem. 2013; 52:6994–6999. [PubMed: 23701462]

[65]. Bhattacharjee A, Andreiadis ES, Chavarot-Kerlidou M, Fontecave M, Field MJ, Artero V. Chemistry – A European Journal. 2013; 19:15166–15174.

[66]. Marinescu SC, Winkler JR, Gray HB. Proceedings of the National Academy of Sciences. 2012; 109:15127–15131.

[67]. Costentin C, Dridi H, Savéant J-M. J. Am. Chem. Soc. 2014; 136:13727–13734. [PubMed: 25190347]

[68]. Dempsey JL, Brunschwig BS, Winkler JR, Gray HB. Acc. Chem. Res. 2009; 42:1995–2004. [PubMed: 19928840]

[69]. Vennampalli M, Liang G, Katta L, Webster CE, Zhao X. Inorg. Chem. 2014; 53:10094–10100. [PubMed: 25247491]

[70]. Scarborough CC, Wieghardt K. Inorg. Chem. 2011; 50:9773–9793. [PubMed: 21678919]

[71]. Savéant J-M. Chem. Rev. 2008; 108:2348–2378. [PubMed: 18620367]

[72]. Leung C-F, Chen Y-Z, Yu H-Q, Yiu S-M, Ko C-C, Lau T-C. Int. J. Hydrogen Energy. 2011; 36:11640–11645.

[73]. Kal S, Filatov AS, Dinolfo PH. Inorg. Chem. 2014; 53:7137–7145. [PubMed: 24963755]

[74]. Mahammed A, Mondal B, Rana A, Dey A, Gross Z. Chem. Commun. 2014; 50:2725–2727.

[75]. Call A, Codolà Z, Acuña-Parés F, Lloret-Fillol J. Chemistry – A European Journal. 2014; 20:6171–6183.

[76]. Costentin C, Savéant J-M. ChemElectroChem. 2014; 1:1226–1236.

[77]. Karunadasa HI, Chang CJ, Long JR. Nature. 2010; 464:1329–1333. [PubMed: 20428167]

[78]. Karunadasa HI, Montalvo E, Sun Y, Majda M, Long JR, Chang CJ. Science. 2012; 335:698–702. [PubMed: 22323816]

[79]. McCrory CCL, Uyeda C, Peters JC. J. Am. Chem. Soc. 2012; 134:3164–3170. [PubMed: 22280515]

[80]. Xie J, Zhou Q, Li C, Wang W, Hou Y, Zhang B, Wang X. Chem. Commun. 2014; 50:6520–6522.

[81]. Goldsmith JI, Hudson WR, Lowry MS, Anderson TH, Bernhard S. J. Am. Chem. Soc. 2005; 127:7502–7510. [PubMed: 15898800]

[82]. Lowry MS, Goldsmith JI, Slinker JD, Rohl R, Pascal RA, Malliaras GG, Bernhard S. Chem. Mater. 2005; 17:5712–5719.

[83]. Dong J, Wang M, Zhang P, Yang S, Liu J, Li X, Sun L. The Journal of Physical Chemistry C. 2011; 115:15089–15096.

[84]. Leung C-F, Ng S-M, Ko C-C, Man W-L, Wu J, Chen L, Lau T-C. Energy Environ. Sci. 2012; 5:7903–7907.

[85]. Guttentag M, Rodenberg A, Bachmann C, Senn A, Hamm P, Alberto R. Dalton Trans. 2013; 42:334–337. [PubMed: 23090353]

[86]. Bachmann C, Guttentag M, Spingler B, Alberto R. Inorg. Chem. 2013; 52:6055–6061. [PubMed: 23641941]

[87]. Bachmann C, Probst B, Guttentag M, Alberto R. Chem. Commun. 2014; 50:6737–6739.

[88]. Lehn JM, Sauvage JP. New J. Chem. 1977; 1:449–451.

[89]. Moradpour A, Amouyal E, Keller P, Kagan H. New J. Chem. 1978; 2:547–549.

[90]. Creaser II, Gahan LR, Geue RJ, Launikonis A, Lay PA, Lydon JD, Mccarthy MG, Mau AWH, Sargeson AM, Sasse WHF. Inorg. Chem. 1985; 24:2671–2680.

[91]. Lay PA, Mau AWH, Sasse WHF, Creaser II, Gahan LR, Sargeson AM. Inorg. Chem. 1983; 22:2347–2349.

[92]. Kirch M, Lehn JM, Sauvage JP. Helv. Chim. Acta. 1979; 62:1345–1384.

[93]. Lehn JM, Ziessel R. Proc. Natl. Acad. Sci. USA. 1982; 79:701–704. [PubMed: 16593151]

[94]. Takizawa, S.-y.; Pérez-Bolívar, C.; Anzenbacher, P.; Murata, S. Eur. J. Inorg. Chem. 2012; 2012:3975–3979.

[95]. Yu Z-T, Yuan Y-J, Cai J-G, Zou Z-G. Chemistry – A European Journal. 2013; 19:1303–1310.

[96]. Yuan Y-J, Yu Z-T, Gao H-L, Zou Z-G, Zheng C, Huang W. Chemistry – A European Journal. 2013; 19:6340–6349.

[97]. Jasimuddin S, Yamada T, Fukuju K, Otsuki J, Sakai K. Chem. Commun. 2010:8466–8468.

[98]. Singh WM, Mirmohades M, Jane RT, White TA, Hammarstrom L, Thapper A, Lomoth R, Ott S. Chem. Commun. 2013; 49:8638–8640.

[99]. Shan B, Baine T, Ma XAN, Zhao X, Schmehl RH. Inorg. Chem. 2013; 52:4853–4859. [PubMed: 23642176]

[100]. Zong R, Thummel RP. J. Am. Chem. Soc. 2005; 127:12802–12803. [PubMed: 16159265]

[101]. Mirmohades M, Pullen S, Stein M, Maji S, Ott S, Hammarström L, Lomoth R. J. Am. Chem. Soc. 2014; 136:17366–17369. [PubMed: 25419868]

[102]. Rodenberg A, Orazietti M, Probst B, Bachmann C, Alberto R, Baldridge KK, Hamm P. Inorg. Chem. 2015 in press.

Europe PMC Funders Author Manuscripts

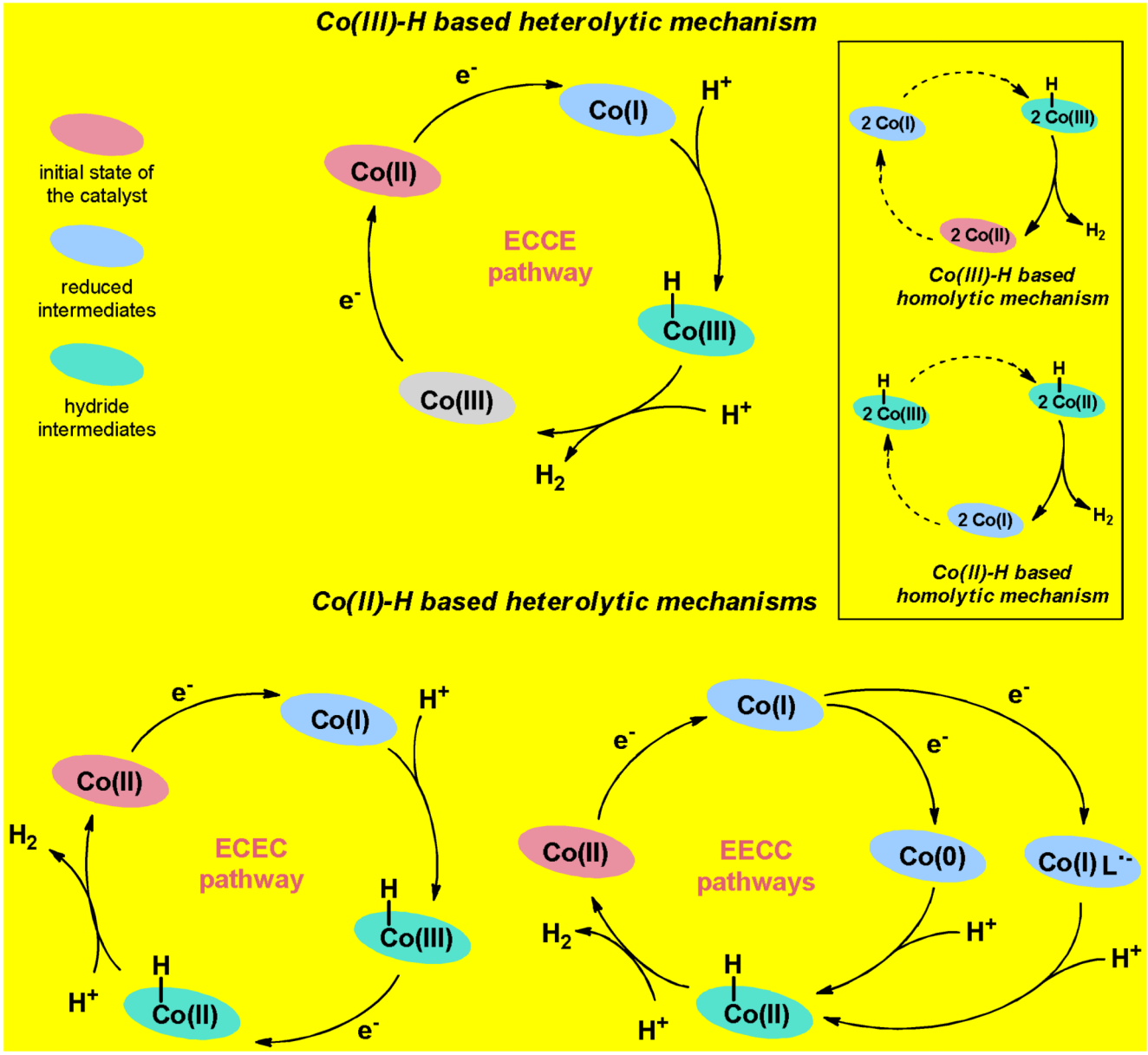

Figure 1.

Heterolytic and homolytic (inset) mechanisms for hydrogen evolution catalyzed by a molecular cobalt(II) complex.

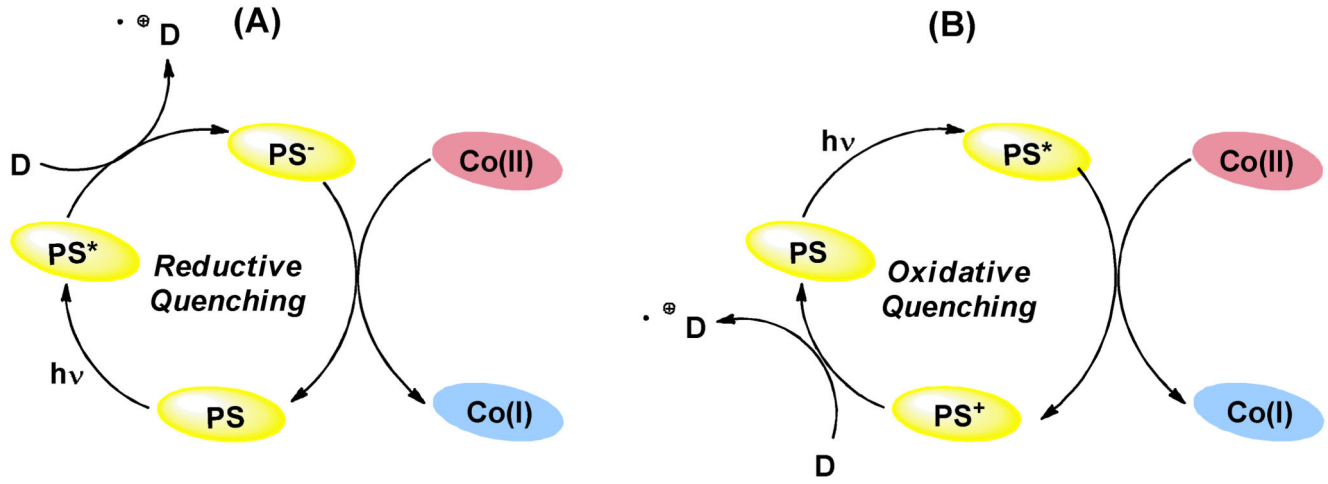

Figure 2.
Photosensitizer-based processes involved in light-driven hydrogen evolution catalyzed by cobalt(II)-polypyridyl complexes.

Europe PMC Funders Author Manuscripts

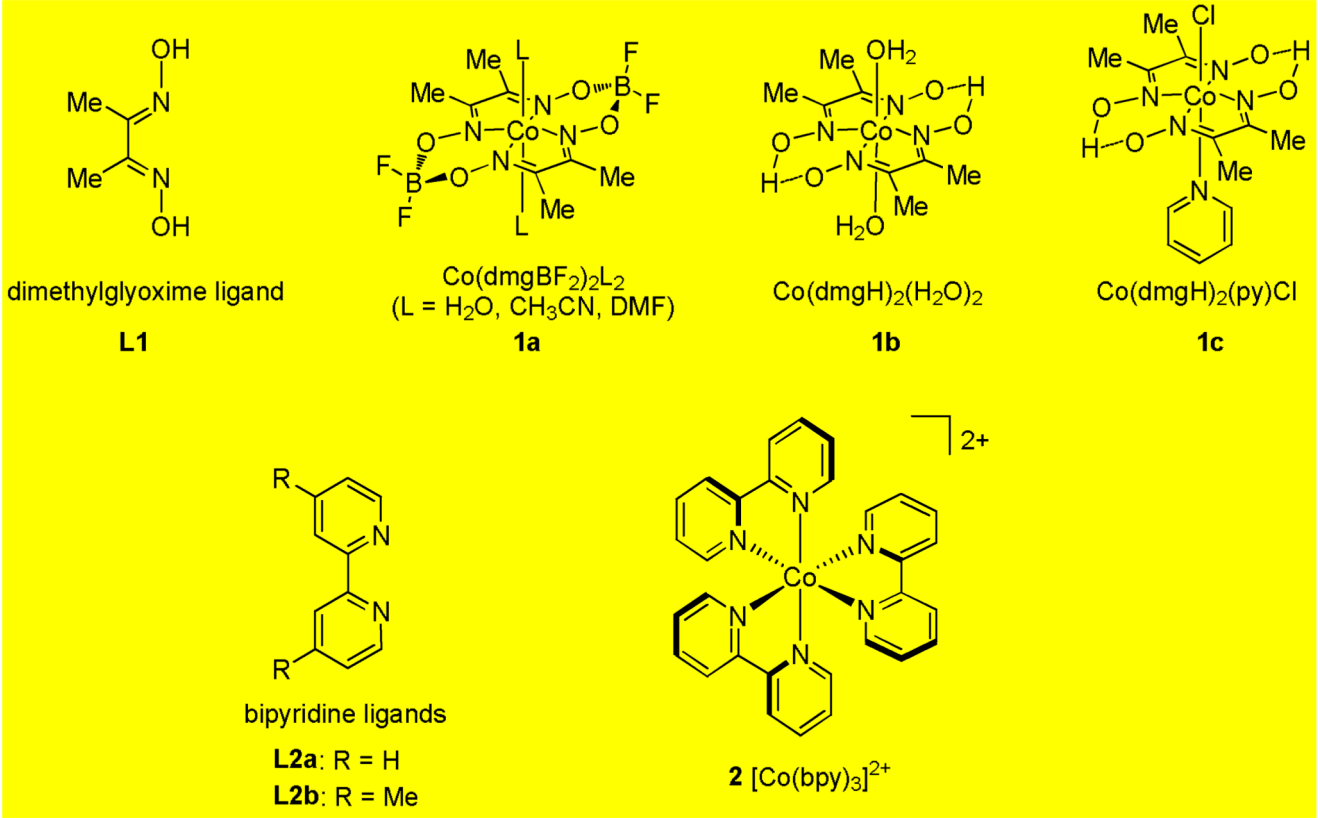

Scheme 1.
Parent cobaloximes and $[Co(bpy)_3]^{2+}$ catalysts.

Europe PMC Funders Author Manuscripts

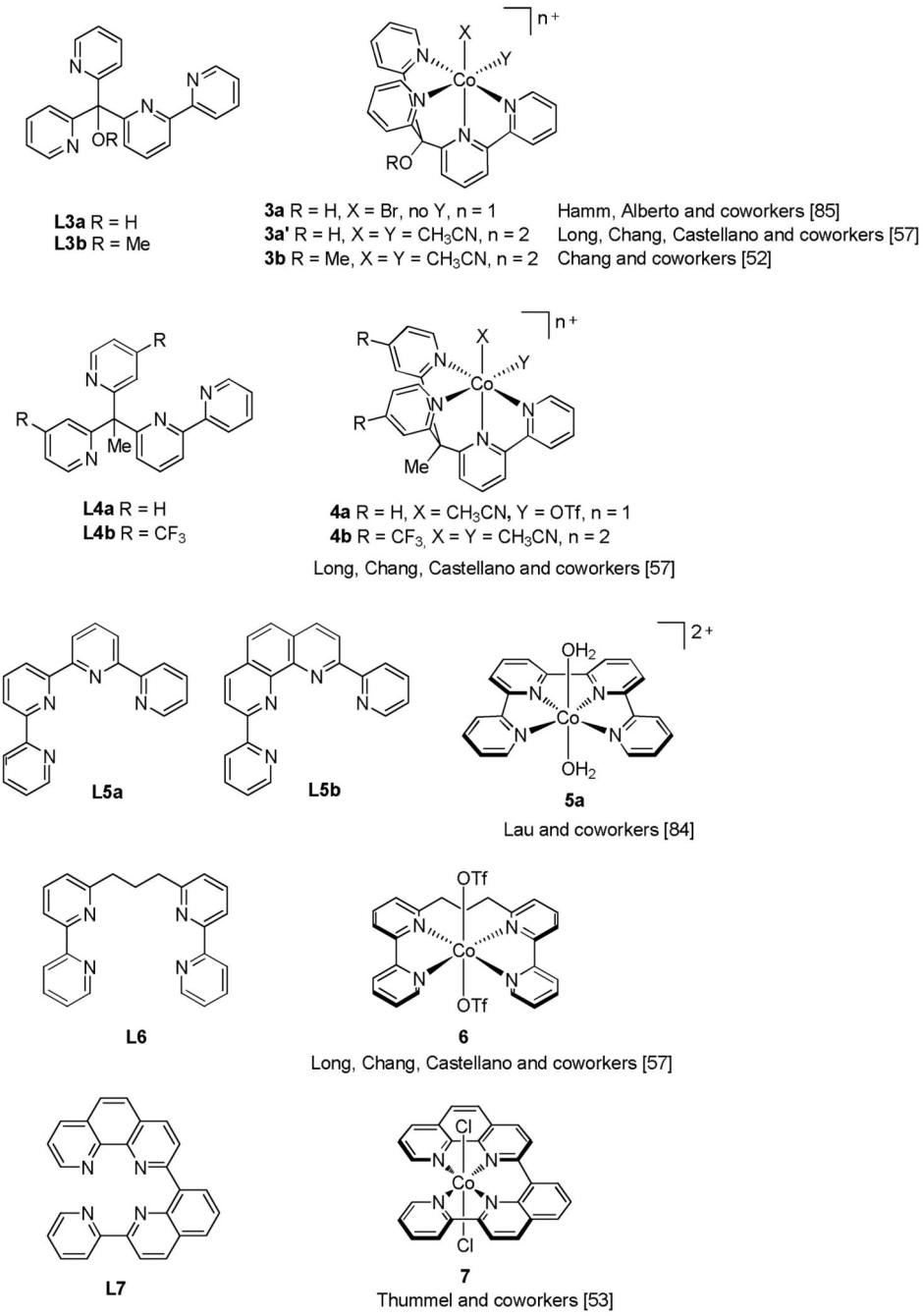

Scheme 2.

Tetradentate bipyridine-based ligands and their corresponding cobalt(II) complexes.

Europe PMC Funders Author Manuscripts

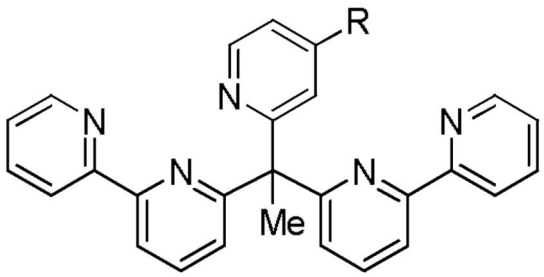

L8a R = H
L8b R = CF_3

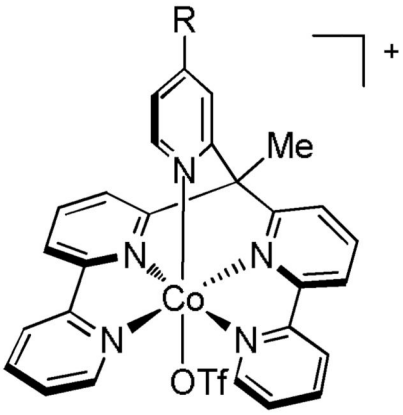

8a R = H
8b R = CF_3

Chang, Castellano, Long and coworkers [54]

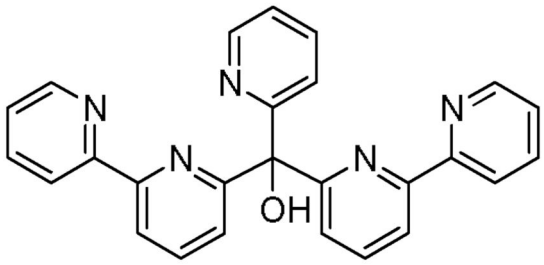

L9

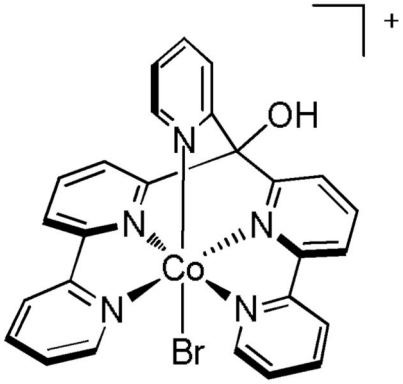

9

Alberto and coworkers [86]

Scheme 3.
Pentadentate bipyridine-based ligands and their corresponding cobalt(II) complexes.

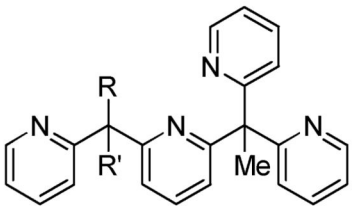

L10a R = R' = H
L10b R = Me, R' = H
L10c R = R '= Me

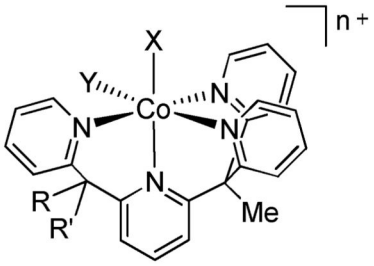

10a R = R' = H, X = CH_3CN, Y = OTf, n = 1
10b R = Me R' = H, X = CH_3CN, Y = OTf, n = 1
10c R = R' = Me, X = CH_3CN, no Y, n = 2

Long, Chang, Castellano and coworkers [57]

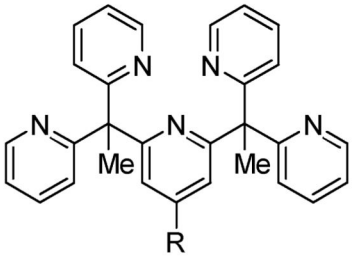

L11a R = CF_3
L11b R = H
L11c R = NMe_2

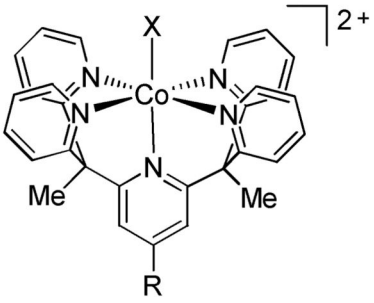

11a R = CF_3, X = H_2O or CH_3CN
11b R = H, X = H_2O or CH_3CN
11c R = NMe_2, X = H_2O or CH_3CN

Long, Chang and coworkers [58]

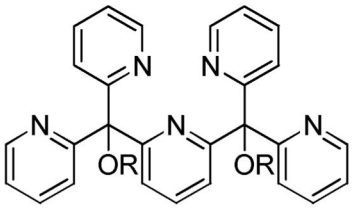

L12a R = H
L12b R = Me

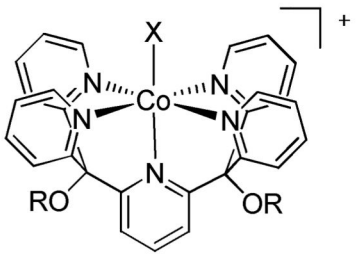

12a R = H, X = Br Alberto and coworkers [86]
12b R = Me, X = Cl Scandola and coworkers [56]

Scheme 4.
Pyridine-based ligands and their corresponding cobalt(II) complexes.

Europe PMC Funders Author Manuscripts

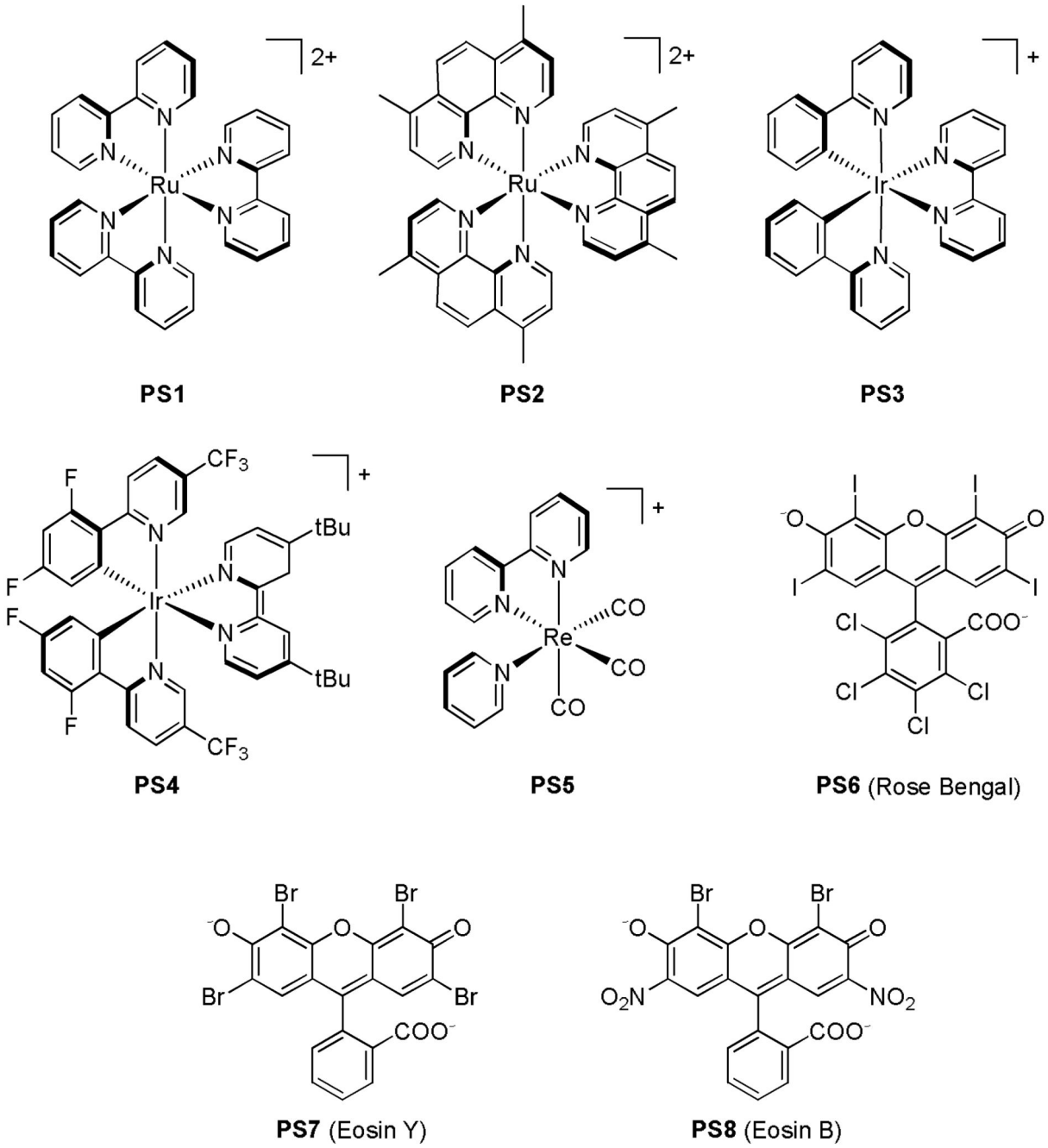

Scheme 5.

Main photosensitizers employed in combination with $[Co(bpy)_3]^{2+}$ (**2**) and cobalt(II)-polypyridyl catalysts.

Europe PMC Funders Author Manuscripts

Table 1

Electrocatalytic performances of hydrogen evolving molecular cobalt(II)-polypyridyl catalysts.

	Conditions				Cyclic Voltammetry			Bulk electrolysis			Ref
	Catalyst	**Electrode**	**Proton source**	**Medium**	**Co(II/I)**	**Electrocatalytic potential**	**Over Potential (±50 mV)**	**Applied Potential (overpotential)**	**TON (reaction time)**	**Faradaic yield**	
Organic electrolytes	**3b**	Glassy carbon	CF_3COOH	CH_3CN(0.1 M nBu_4NPF_6)	−0.81 V *vs* SCE	−0.81 V *vs* SCE (mid-wave)	400 mV	−1 V *vs* SCE	n.i.	99%	[52]
	3b	Glassy carbon	CF_3COOH	0.1 M KNO_3 in H_2O/ CH_3CN 1:1	−1 V *vs* SCE	−1 V *vs* SCE (mid-wave)	–	–	–	–	[52]
	7	Glassy carbon	–	DMF (0.1 M nBu_4NPF_6)	−0.53 V *vs* SCE	–	–	–	–	–	[53]
	8a	Glassy carbon	CH_3COOH	CH_3CN(0.1 M nBu_4NPF_6)	−1.20 V *vs* Fc^+/Fc	−1.72 & −1.83V *vs* Fc^+/Fc (mid-wave)	530 mV	n.i.	n.i.	90%	[54]
	8b	Glassy carbon	CH_3COOH	CH_3CN(0.1 M nBu_4NPF_6)	−1.14 V *vs* Fc^+/Fc	−1.60 & −1.85V *vs* Fc^+/Fc (mid-wave)	460 mV	n.i.	n.i.	90%	[54]
	11b	Glassy carbon	CH_3COOH[a]	CH_3CN(0.1 M nBu_4NPF_6)	−1.47 V *vs* Fc^+/Fc[b]	−1.74 V *vs* Fc^+/Fc (mid wave)	500 mV	n.i.	n.i.	100%	[55]
	12b	Glassy carbon	CF_3COOH	CH_3CN(0.1 M $LiClO_4$)	−1.31 V *vs* SCE	−1.31V *vs* SCE (mid wave)	–	–	–	–	[56]
Fully aqueous electrolytes	**4a**	Glassy carbon	H_2O	Ascorbate buffer 0.3 M, pH 4	−0.9 V *vs* SHE	−0.9 V *vs* SHE (onset)	–	–	–	–	[57]
	7	Glassy carbon	H_2O	Phosphate buffer, pH 7	−0.4 V *vs* SHE	−0.9 V *vs* SHE (onset)	480 mV	–	–	–	[53]
	8a	Glassy carbon	H_2O	Ascorbate buffer 0.3 M, pH 4	−0.85 V *vs* SHE	–	–	–	–	–	[54]
	10a	Glassy carbon	H_2O	Ascorbate 0.3 M, pH 7	−1.0 V *vs* SHE	−1.0 V *vs* SHE (onset)		−1.20 V *vs* SHE	60 (3h)	100%	[57]
	10b	Glassy carbon	H_2O	Ascorbate 0.3 M, pH 7	−1.0 V *vs* SHE	−1.0 V *vs* SHE (onset)		−1.20 V *vs* SHE	40 (3h)	100%	[57]
	10c	Glassy carbon	H_2O	Ascorbate 0.3 M, pH 7	−0.8 v *vs* SHE	−0.8 V *vs* SHE (onset)		−1.20 V *vs* SHE	~0 (3h)	-	[57]
	11a	Hg pool	H_2O	2 M Phosphate buffer, pH 7	−0.84 V *vs* SHE	−0.84 V *vs* SHE & −1.00 V *vs* SHE	420 mV	–	–	–	[58]

Europe PMC Funders Author Manuscripts

Conditions				Cyclic Voltammetry			Bulk electrolysis			Ref
Catalyst	Electrode	Proton source	Medium	Co(II/I)	Electrocatalytic potential	Over Potential (±50 mV)	Applied Potential (overpotential)	TON (reaction time)	Faradaic yield	
11a	Glassy carbon (RDE)	H_2O	0.1 M Phosphate buffer, pH 7	–	–	–	−0.963 V *vs* SHE (550 mV)	–	95%	[59]
11b	Hg pool	H_2O	2 M Phosphate buffer, pH 7	−1.00 V *vs* SHE	−1.00 V *vs* SHE & −1.20 V *vs* SHE	660 mV	−1.30 V *vs* SHE	55 000 (60 h)	100%	[58]
11c	Hg pool	H_2O	2 M Phosphate buffer, pH 7	−1.12 V *vs* SHE	−1.12 V *vs* SHE & −1.30 V *vs* SHE	–	–	–	–	[58]

[a] Anation process.

[b] Converted from $E(Fc^+/Fc)$ = +0.64 V *vs* SHE.

Europe PMC Funders Author Manuscripts

Table 2

Photocatalytic performances of homogeneous systems based on hydrogen evolving $[Co(bpy)_3]^{2+}$ and cobalt(II)–polypyridyl catalysts.

	Cat	[Cat]	PS	Ratio PS : Cat	Conditions	pH	Light	Irr. Time	Amount of H_2	TON (H_2/Co)	TOF (h^{-1})	Φ	Ref.
Organic and mixed organic/aqueous medium	**2**	5 mM	**PS_2**	1 : 20	CH_3CN/H_2O, 1:1 TEOA (0.5 M) LiCl (0.25 M)	8.0	≥ 400 nm	–	–	–	–	29%	[48]
	2	2.5 mM	**PS_1**	1 : 50	CH_3CN/H_2O, 1:1 TEOA (0.57 M) LiCl (0.27 M)	_ [a]	LED 465 nm	o/n	50 μmol	2	–	–	[81]
	2	2.5 mM	**PS_2**	1 : 50	CH_3CN/H_2O, 1:1 TEOA (0.57 M) LiCl (0.27 M)	_ [a]	LED 465 nm	o/n	290 μmol	12	–	–	[81]
	2	2.5 mM	**PS_3**	1 : 50	CH_3CN/H_2O, 1:1 TEOA (0.57 M) LiCl (0.27 M)	_ [a]	LED 465 nm	o/n	400 μmol	16	–	–	[81]
	2	5 mM	**PS_2**	1 : 33	CH_3CN/H_2O, 1:1 TEOA (0.57 M) LiCl (0.27 M)	_ [b]	LED 465 nm	40 h	145 μmol	2.9 [c]	–	–	[82]
	2	5 mM	**PS_4**	1 : 33	CH_3CN/H_2O, 1:1 TEOA (0.57 M) LiCl (0.27 M)	_ [b]	LED 465 nm	40 h	265 μmol	5.3 [c]	–	–	[82]
	2	0.4 mM	**PS_6**	1 : 1	CH_3CN/H_2O, 1:1 TEA (10% v/v)	10	> 450 nm	2 h	382 μmol	191	–	–	[83]
	2	40 μM	**PS6**	10 : 1	CH_3CN/H_2O, 1:1 TEA (10% v/v)	10	>450 nm	2 h	126 μmol	631	–	–	[83]
	2	0.6 mM	**PS_3**	1 : 20	CH_3CN, TEOA (0.2 M) p-cyanoanilinium (0.025 M)	–	>390 nm	20 h	72 μmol	12 [c]	–	–	[84]
	$[Co(bpy)_2(OH_2)_2]^{2+}$	0.6 mM	**PS_3**	1 : 20	CH_3CN, TEOA (0.2 M) p-cyanoanilinium (0.025 M)	–	> 390 nm	20 h	66 μmol	11 [c]	–	–	[84]
	5a	0.6 mM	**PS_3**	1 : 20	CH_3CN, TEOA (0.2 M) p-cyanoanilinium (0.025 M)	–	> 390 nm	20 h	162 μmol	27 [c]	–	–	[84]
	5a	0.6 mM	**PS_4**	1 : 20	CH_3CN, TEOA (0.2 M)	–	> 420 nm	20 h	306 μmol	51 [c]	–	–	[84]

Europe PMC Funders Author Manuscripts

	Cat	[Cat]	PS	Ratio PS : Cat	Conditions	pH	Light	Irr. Time	Amount of H_2	TON (H_2/Co)	TOF (h^{-1})	Φ	Ref.
					p-cyanoanilinium (0.025 M)								
	5a	0.6 mM	**PS_4**	1 : 20	CH_3CN/H_2O, 95:5 TEOA (0.2 M) p-cyanoanilinium (0.025 M)	–	> 420 nm	20 h	348 µmol	58[C]	–	–	[84]
	5a	0.6 mM	**PS_4**	1 : 20	CH_3CN/H_2O, 95:5 TEOA (0.2 M)	–	> 420 nm	20 h	270 µmol	45[C]	–	–	[84]
Fully aqueous medium	**L2a + Co(II)**	2 mM **L2a** + 10 mM Co(II)	**PS1**	min. 1 : 4	H_2A/HA^- (0.7 M)	5.0	Visible light	1-3 h	–	–	–	2%	[45]
	L2b + Co(II)	2 mM **L2b** + 10 mM Co(II)	**PS1**	min. 1 : 4	H_2A/HA^- (0.7 M)	5.0	Visible light	1-3 h	–	–	–	13%	[45]
	3a	0.1 µM	**PS5**	5000 : 1	H_2A/HA^- (1 M)	4.1	LED 385 nm	20 h	30 µmol	9000	–	–	[85]
	3a	0.5 mM	**PS5**	1 : 16.7	H_2A/HA^- (1 M)	4.1	LED 385 nm	120 h	520 µmol	104[C]	–	–	[85]
	3a'	20 µM	**PS1**	16.5 : 1	H_2A/HA^- (0.3 M)	4.0	LED 452 nm	14 h	190 µmol	950[C]	–	–	[57]
	3b	20 µM	**PS1**	16.5 : 1	H_2A/HA^- (0.3 M)	4.5	LED 452 nm	14 h	205 µmol	1025[C]	–	–	[57]
	4a	40 µM	**PS1**	8.25 : 1	H_2A/HA^- (0.5 M)	4.0	LED 452 nm	–	–	–	–	7.5 ± 0.8%	[57]
	4a	1 µM	**PS1**	330 : 1	H_2A/HA^- (0.3 M)	4.0	Simulated Sunlight (100 $mW.cm^{-2}$)	2.5 h	–	~4200	~3160	–	[57]
	4a	20 µM	**PS1**	16.5 : 1	H_2A/HA^- (0.3 M)	4.0	LED 452 nm	14 h	370 µmol	1850[C]	–	–	[57]
	4b	20 µM	**PS1**	16.5 : 1	H_2A/HA^- (0.3 M)	4.5	LED 452 nm	14 h	80 µmol	400[C]	–	–	[57]
	5a	20 µM	**PS1**	16.5 : 1	$H2_A/HA^-$ (0.3 M)	5.5	LED 452 nm	14 h	40 µmoL	200[C]	–	–	[57]

Europe PMC Funders Author Manuscripts

	Cat	[Cat]	PS	Ratio PS : Cat	Conditions	pH	Light	Irr. Time	Amount of H_2	TON (H_2/Co)	TOF (h^{-1})	Φ	Ref.
	6	20 μM	**PS1**	16.5 : 1	H_2A/HA^- (0.3 M)	5.0	LED 452 nm	14 h	30 μmoL	150[c]	–	–	[57]
	7	3 μM	**PS1**	133 : 1	H_2A/HA^- (0.3 M)	4.0	LED 469 nm	3 h	10 μmoL	333	586	–	[53]
	8a	20 μM	**PS1**	16.5 : 1	H_2A/HA^- (0.3 M)	4.0	LED 452 nm	13 h	326 μmol[d]	1630	660	3.6%	[54]
	8b	20 μM	**PS1**	16.5 : 1	H_2A/HA^- (0.3 M)	4.5	LED 452 nm	13 h	278 μmol[d]	1390	500	2.7%	[54]
	9	0.1 μM	**PS5**	5000 : 1	H_2A/HA^- (1 M)	4.1	LED 385 nm	–	–	10800	–	–	[86]
	9	5 μM	**PS5**	100 : 1	H_2A/HA^- (1 M)	4.1	LED 385 nm	15 h	69 μmol	1380	920	–	[86]
	9	1 μM	**PS1**	500 : 1	H_2O, TCEP[e] (0.1 M) NaHA (100 mM)	5.0	LED 385 nm	11 h	290 μmol	33300	5900	–	[87]
	9	100 μM	**PS1**	5 : 1	H_2O, TCEP[e] (0.1 M) NaHA (100 mM)	5.0	LED 385 nm	35 h	970 μmol	1080	70	–	[87]
	10a	20 μM	**PS1**	16.5 : 1	H_2A/HA^- (0.3 M)	5.0	LED 452 nm	–	310 μmol[d]	1550	–	–	[57]
	10a	1.25 μM	**PS1**	264 : 1	H_2A/HA^- (0.3 M)	7.0	LED 452 nm	–	–	2400	–	–	[57]
	10b	20 μM	**PS1**	16.5 : 1	H_2A/HA^- (0.3 M)	5.5	LED 452 nm	–	50 μmol[d]	250	–	–	[57]
	10c	20 μM	**PS1**	16.5 : 1	H_2A/HA^- (0.3 M)	5.0	LED 452 nm	–	45 μmol[d]	225	–	–	[57]
	11a	250 μM	**PS1**	1 : 1.25	Phosphate buffer (1 M) H_2A/HA^- (0.1 M)	7.0	≥ 455 nm	2 h	–	–	–	0.6%	[59]
	11a	50 μM	**PS1**	4 : 1	Phosphate buffer (1 M) H_2A/HA^- (0.1 M)	7.0	≥ 455 nm	8 h	0.50 mL	–	–	–	[59]
	11a	20 μM	**PS1**	16.5 : 1	H_2A/HA^- (0.3 M)	6.0	LED 452 nm	13 h	~60 μmol	~300	–	–	[54]
	11b	50 μM	**PS1**	4 : 1	Phosphate buffer (1 M) H_2A/HA^- (0.1 M)	7.0	≥455 nm	8 h	0.42 mL	–	–	–	[59]

Europe PMC Funders Author Manuscripts

	Cat	[Cat]	PS	Ratio PS : Cat	Conditions	pH	Light	Irr. Time	Amount of H_2	TON (H_2/Co)	TOF (h^{-1})	Φ	Ref.
	11b	20 µM	**PS1**	16.5 : 1	H_2A/HA^- (0.3 M)	6.0	LED 452 nm	13 h	~60 µmol	~300	–	–	[54]
	11c	50 µM	**PS1**	4 : 1	Phosphate buffer (1 M) H_2A/HA^- (0.1 M)	7.0	≥455 nm	8 h	0.25 mL	–	–	–	[59]
	12a	5 µM	**PS5**	100 : 1	H_2A/HA^- (1 M)	4.1	LED 385 nm	40 h	59 µmol	1180	–	–	[86]
	12b	50 µM	**PS1**	10 : 1	Acetate buffer (1 M) H_2A/HA^- (0.1 M)	4.0	>400 nm	1 h	45 µmol	187	486	–	[56]

[a] pH adjusted by addition of 0.4 mL of 12 M HCl.

[b] pH adjusted by addition of 0.125 mL of 37% HCl.

[c] TON(H_2/Co) not given in the reference paper but calculated from the reported TON(PS) or from the reported amount of produced hydrogen.

[d] Amount of hydrogen calculated from the reported TON value, the catalyst concentration and the solution volume.

[e] Tris(2-carboxylethyl)phosphine (TCEP).